

MODELING WELL PERFORMANCE IN COMPARTMENTALIZED GAS  
RESERVOIRS

A Thesis

by

NURUDEEN YUSUF

Submitted to the Office of Graduate Studies of  
Texas A&M University  
in partial fulfillment of the requirements for the degree of

MASTER OF SCIENCE

December 2007

Major Subject: Petroleum Engineering

NURUDEEN YUSUF

A Thesis

by

NURUDEEN YUSUF

Submitted to the Office of Graduate Studies of  
Texas A&M University  
in partial fulfillment of the requirements for the degree of

MASTER OF SCIENCE

Approved by:

Chair of Committee, Robert A. Wattenbarger  
Committee Members, James B. Maggard  
Yalchin Efendiev

Head of Department, Steven A. Holditch

December 2007

Major Subject: Petroleum Engineering

## ABSTRACT

Modeling Well Performance in Compartmentalized Gas Reservoirs.

(December 2007)

Nurudeen Yusuf, B.S., University of Lagos

Chair of Advisory Committee: Dr. Robert A. Wattenbarger

Predicting the performance of wells in compartmentalized reservoirs can be quite challenging to most conventional reservoir engineering tools. The purpose of this research is to develop a Compartmentalized gas Depletion Model that applies not only to conventional consolidated reservoirs (with constant formation compressibility) but also to unconsolidated reservoirs (with variable formation compressibility) by including geomechanics, permeability deterioration and compartmentalization to estimate the OGIP and performance characteristics of each compartment in such reservoirs given production data.

A geomechanics model was developed using available correlation in the industry to estimate variable pore volume compressibility, reservoir compaction and permeability reduction. The geomechanics calculations were combined with gas material balance equation and pseudo-steady state equation and the model was used to predict well performance.

Simulated production data from a conventional gas Simulator was used for consolidated reservoir cases while synthetic data (generated by the model using known

parameters) was used for unconsolidated reservoir cases. In both cases, the Compartmentalized Depletion Model was used to analyze data, and estimate the *OGIP* and  $J_g$  of each compartment in a compartmentalized gas reservoir and predict the subsequent reservoir performance. The analysis was done by history-matching gas rate with the model using an optimization technique.

The model gave satisfactory results with both consolidated and unconsolidated reservoirs for single and multiple reservoir layers. It was demonstrated that for unconsolidated reservoirs, reduction in permeability and reservoir compaction could be very significant especially for unconsolidated gas reservoirs with large pay thickness and large depletion pressure.

## DEDICATION

This thesis is dedicated to God almighty, my wife: Temiloluwa and members of my extended family.

## ACKNOWLEDGEMENTS

I would like to thank my committee chair, Dr. Wattenbarger, and my committee members, Dr. Maggard and Dr. Effendiev for their guidance and support throughout the course of this research. Thanks also go to my friends and colleagues and the department, faculty and staff for making my time at Texas A&M University a great experience. Finally, thanks to my wife for her patience and love.

## TABLE OF CONTENTS

	Page
ABSTRACT .....	iii
DEDICATION .....	v
ACKNOWLEDGEMENTS .....	vi
TABLE OF CONTENTS .....	vii
LIST OF FIGURES.....	ix
LIST OF TABLES .....	xii
1. INTRODUCTION	
1.1 Problem Description.....	1
1.2 Literature Review .....	2
1.3 Objectives and Procedures .....	9
2. COMPARTMENTALIZED DEPLETION MODEL	
2.1 Gas Depletion Calculations.....	11
2.2 Model Notation .....	13
2.3 Model's Calculations for Single-Layer Case .....	15
2.4 Model's Calculations for Multiple-Layer Case.....	18
2.5 Model's Calculations for Entire Field.....	20
2.6 Data Input and Output .....	21
2.7 Running the Model.....	22
2.8 Model's Assumptions.....	22
3. RESULTS WITH CONSOLIDATED RESERVOIRS	
3.1 Single-Layer Conventional Consolidated Reservoir.....	24
3.2 Multi-Layer Conventional Consolidated Reservoir .....	34

4. RESULTS WITH UNCONSOLIDATED RESERVOIRS	
4.1 Single-Layer Deep water Unconsolidated Reservoir .....	40
4.2 Multi-Layer Deep water Unconsolidated Reservoir .....	50
5. DISCUSSIONS	
5.1 Status of Model .....	57
5.2 Limitation of Model .....	57
5.3 Timeframe of Production Data.....	58
6. RESULTS WITH UNCONSOLIDATED RESERVOIRS	
6.1 Conclusions .....	59
6.2 Recommendations .....	60
NOMENCLATURE.....	61
REFERENCE.....	64
APPENDIX A: Basic Geomechanics.....	68
APPENDIX B: Measurement of Variable Formation Compressibility .....	72
VITA .....	75

## LIST OF FIGURES

	Page
Figure 1.1 Formation Compressibility using Yale's Correlation .....	8
Figure 2.1 A Typical One Layer Model .....	15
Figure 2.2 A Typical 2-Layer Model with Crossflow .....	18
Figure 3.1 Average Reservoir Pressure Vs Time for 1-Layer Consolidated Reservoir Case A before Optimization .....	28
Figure 3.2 Gas Rate Vs Time for 1-Layer Consolidated Reservoir Case A before Optimization .....	28
Figure 3.3 Average Reservoir Pressure Vs Time for 1-Layer Consolidated Reservoir Case A after Optimization .....	29
Figure 3.4 Gas Rate Vs Time for 1-Layer Consolidated Reservoir Case A after Optimization .....	29
Figure 3.5 Average Reservoir Pressure Vs Time for Consolidated 1-Layer Case B after Optimization .....	30
Figure 3.6 Gas Rate Vs Time for 1-Layer Consolidated Reservoir Case B after Optimization .....	30
Figure 3.7 Average Reservoir Pressure Vs Time for 1-Layer Consolidated Reservoir Case D after Optimization .....	31
Figure 3.8 Gas Rate Vs Time for 1-Layer Consolidated Reservoir Case D after Optimization .....	31
Figure 3.9 Average Reservoir Pressure Vs Time for 1-Layer Consolidated Reservoir Case A Including Transient data in Optimization .....	32
Figure 3.10 Gas Rate Vs Time for 1-Layer Consolidated Reservoir Case A Including Transient data in Optimization .....	32
Figure 3.11 Gas Rate Vs Time for 2-Layer Consolidated Reservoir Case C-D after Optimization .....	36

Figure 3.12 Gas Rate $V_s$ Time for 3-Layer Consolidated Reservoir Case <i>C-D</i> after Optimization .....	37
Figure 3.13 Gas Rate $V_s$ Time for 4-Layer Consolidated Reservoir Case <i>B-C-D</i> after Optimization .....	38
Figure 3.14 Gas Rate $V_s$ Time for 5-Layer Consolidated Reservoir Case <i>A-B-C-D-E</i> after Optimization .....	39
Figure 4.1 Average Reservoir Pressure $V_s$ Time for 1-Layer Unconsolidated Reservoir Case <i>A</i> after Optimization.....	43
Figure 4.2 Gas Rate $V_s$ Time for 1-Layer Unconsolidated Reservoir Case <i>A</i> after Optimization .....	43
Figure 4.3 Reservoir Height Variation and Compaction $V_s$ Average Reservoir Pressure for 1-Layer Unconsolidated Reservoir Case <i>A</i> .....	44
Figure 4.4 Permeability Variation $V_s$ Average Reservoir Pressure for 1-Layer Unconsolidated Reservoir Case <i>A</i> .....	44
Figure 4.5 Average Reservoir Pressure $V_s$ Time for 1-Layer Unconsolidated Reservoir Case <i>D</i> after Optimization .....	45
Figure 4.6 Gas Rate $V_s$ Time for 1-Layer Unconsolidated Reservoir Case <i>D</i> after Optimization .....	45
Figure 4.7 Reservoir Height Variation and Compaction $V_s$ Average Reservoir Pressure for 1-Layer Unconsolidated Reservoir Case <i>D</i> .....	46
Figure 4.8 Permeability Variation $V_s$ Average Reservoir Pressure for 1-Layer Unconsolidated Reservoir Case <i>D</i> .....	46
Figure 4.9 Average Reservoir Pressure $V_s$ Time for 1-Layer Unconsolidated Reservoir Case <i>E</i> after Optimization.....	47
Figure 4.10 Gas Rate $V_s$ Time for 1-Layer Unconsolidated Reservoir Case <i>E</i> after Optimization.....	47
Figure 4.11 Reservoir Height Variation and Compaction $V_s$ Average Reservoir Pressure for 1-Layer Unconsolidated Reservoir Case <i>E</i> .....	48
Figure 4.12 Permeability Variation $V_s$ Average Reservoir Pressure for 1-Layer Unconsolidated Reservoir Case <i>E</i> .....	48

Figure 4.13 Gas Rate $V_s$ Time for 2-Layer Unconsolidated Reservoir Case <i>A-B</i> after Optimization.....	51
Figure 4.14 Reservoir Compaction $V_s$ Average Reservoir Pressure for 2-Layer Unconsolidated Reservoir Case <i>A-B</i> .....	52
Figure 4.15 Permeability Variation $V_s$ Average Reservoir Pressure for 2-Layer Unconsolidated Reservoir Case <i>A-B</i> .....	52
Figure 4.16 Gas Rate $V_s$ Time for 2-Layer Unconsolidated Reservoir Case <i>A-C</i> after Optimization.....	53
Figure 4.17 Reservoir Compaction $V_s$ Average Reservoir Pressure for 2-Layer Unconsolidated Reservoir Case <i>A-C</i> .....	54
Figure 4.18 Permeability Variation $V_s$ Average Reservoir Pressure for 2-Layer Unconsolidated Reservoir Case <i>A-C</i> .....	54
Figure 4.19 Gas Rate $V_s$ Time for 3-Layer Unconsolidated Reservoir Case <i>A-B-C</i> after Optimization .....	55
Figure 4.20 Compaction $V_s$ Average Reservoir Pressure for 3-Layer Unconsolidated Reservoir Case <i>A-B-C</i> .....	56
Figure 4.21 Permeability Variation $V_s$ Average Reservoir Pressure for 3-Layer Unconsolidated Reservoir Case <i>A-B-C</i> .....	56
Figure A.1 Stress / Pressure Balance on Formation before Production .....	68
Figure A.2 Stress / Pressure Balance on Formation during Production .....	69
Figure B.1 Oedometer Test .....	71
Figure B.2 Hydrostatic Test .....	72

## LIST OF TABLES

	Page
Table 1.1 Constants for different Rocks in Yale's Correlation.....	7
Table 2.1 A Typical Array of Productivity Indices.....	14
Table 2.2 A Typical array of Flux Coefficients .....	14
Table 3.1 Reservoir Properties for Consolidated Reservoirs .....	25
Table 3.2 Properties for different Consolidated Reservoir Layers.....	25
Table 3.3 Comparison between Model and Simulator Results for 1-Layer Consolidated Reservoir Case A.....	33
Table 3.4 Comparison between Model and Simulator Results for 1-Layer Consolidated Reservoir Case B.....	33
Table 3.5 Comparison between Model and Simulator Results for 1-Layer Consolidated Reservoir Case D.....	33
Table 3.6 Comparison between Model and Simulator Results for 2-Layer Consolidated Reservoir Case C-D.....	36
Table 3.7 Comparison between Model and Simulator Results for 3-Layer Consolidated Reservoir Case B-C-D.....	37
Table 3.8 Comparison between Model and Simulator Results for 4-Layer Consolidated Reservoir Case A-B-C-D .....	38
Table 3.9 Comparison between Model and Simulator Results for 5-Layer Consolidated Reservoir Case A-B-C-D-E .....	39
Table 4.1 Reservoir Properties for Unconsolidated Reservoir .....	41
Table 4.2 Properties for different Unconsolidated Reservoir Layers.....	41
Table 4.2b Guess Values used in running the Model for Single or Multiple Layered Cases .....	42

Table 4.3	Comparison between Model and Synthetic data for 1-Layer Unconsolidated Reservoir Case <i>A</i> .....	49
Table 4.4	Comparison between Model and Synthetic data for 1-Layer Consolidated Reservoir Case <i>D</i> .....	49
Table 4.5	Comparison between Model and Synthetic data for 1-Layer Consolidated Reservoir Case <i>E</i> .....	49
Table 4.6	Comparison between Model and Synthetic data for 2-Layer Consolidated Reservoir Case <i>A-B</i> .....	51
Table 4.7	Comparison between Model and Synthetic data for 2-Layer Consolidated Reservoir Case <i>A-C</i> .....	53
Table 4.8	Comparison between Model and Synthetic data for 3-Layer Consolidated Reservoir Case <i>A-B-C</i> .....	55
Table 5.1	Status of Depletion Model.....	57

## 1. INTRODUCTION

### 1.1 Problem Description

Early versions of reservoir performance predictive tools incorporated reservoir description in a manner which was consistent with the technology of the times. Conventional tools generally employ constant pore compressibility to account for porosity and permeability changes. These assumptions are inadequate in *HPHT* deep water reservoirs due to geomechanical stresses. Peculiar issues to unconsolidated *HPHT* reservoirs such as reservoir compaction and surface subsidence are also largely unaccounted for in conventional tools. This problem is even more complicated in compartmentalized *HPHT* reservoirs.

In comparison to Land or shallow-water reservoirs, deep-water reservoirs are located at great depth below the seafloor varying from 500m (deep-water) to 2000 m and beyond (Ultra-deep). They therefore have less overburden; they are geo-pressured and highly unconsolidated. Typically the rock compressibility of deep-water sands could be up to 50 micro sips<sup>1</sup> which is about 10 times the normal range for consolidated sands. Formation compressibility higher than 100 micro sips have been measured experimentally<sup>2</sup>. Formation compressibility for unconsolidated rocks also reduces significantly with depletion. These characteristics (high rock compressibility which reduces with pressure) implies that pore volume, porosity and permeability could vary

---

This thesis follows the style of *Society of Petroleum Engineers*

significantly leading to reservoir compaction, well stability issues and surface subsidence<sup>3</sup>.

For instance, in an experiment conducted by Ostermeier<sup>4-5</sup> on cores samples from Deep- water Gulf of Mexico in 2001, a pressure depletion of 7,000 psi produced a 25% reduction in porosity and 85% reduction in permeability. Field cases of permeability reduction and reservoir compaction have also been reported by other authors<sup>6-9</sup>.

Modeling such reservoirs with conventional engineering tools based on constant pore compressibility would therefore give inaccurate results, leading to inaccurate reserve estimation and false projected economics. The main method available in handling unconsolidated deep-water resources is coupling commercial reservoir simulators with geomechanics simultaneously. This method is generally too expensive and time consuming to be available as a common tool on all conventional reservoir simulation packages.

## 1.2 Literature Review

The most common methods of analyzing and interpreting gas production data in wells completed in single or multi-layered reservoirs include decline curve analysis and Layered PSS modeling (a combination of material balance and *PSS* calculations). The following summarizes major work in these methods and also mentions some advances in geomechanics as it relates to reservoir performance.

Decline Curve Analysis is a common method of estimating *OGIP* and predicting ultimate gas reserves at a future abandonment pressure based on the assumption that future production will follow a past trend. The original form introduced by Arps<sup>10</sup> employs an empirical relationship between rate and time to represent production decline in a well or in an entire field. The characteristic of Arp's equation is captured by the decline exponent  $b$ . Depending on the value of  $b$ , the form of the equation could be exponential ( $b = 0$ ), hyperbolic ( $0 < b < 1$ ) or harmonic ( $b = 1$ ). The characteristic shape of each curve either on Cartesian or semi log graphs of  $q_g$  Vs  $t$  and  $q_g$  Vs  $G_p$  can help identify each type. This method is only applicable to boundary dominated flow without non Darcy flow effect.

The hyperbolic case of Arp's equation does not have a linear shape on either the Cartesian or the Log-log plots and requires the use of a trial and error method to evaluate production data. Type curves were developed using theoretical considerations to eliminate the trial and error analysis of Arp's curves. Their application requires that the shape of field data is matched with a type curve to predict field performance.

Fetkovich Decline Type Curves<sup>11</sup> is based on analytical solutions to flow equations for production at constant *BHP* and include both transient and boundary dominated flow periods. These log-log curves are plotted in terms of dimensionless variables and can be used to estimate *OGIP*, production forecast and reservoir properties through type curve matching techniques. The Fetkovich type curves however assume constant fluid viscosity and compressibility as they were developed to model a slightly compressible

fluid. This assumption is not valid gas flow under boundary dominated especially at high drawdown.

In order to improve the accuracy of Fetkovich type curve for analyzing gas wells with large pressure drawdown, Carter <sup>12</sup> defined plotting functions that consider the variation of gas properties (viscosity and compressibility) with average reservoir pressure by defining dimensionless variables in terms of real gas pseudo-pressure function. He related  $q_g(t)/t$  behavior during boundary dominated flow with a parameter  $\lambda$ , which varies from 0.5 to 1. The  $\lambda = 1$  represents the liquid case and corresponds to Arps exponential decline case.

One of the limitations of Conventional Decline Curve Analysis applied to either single or multiple-layered gas reservoirs is that production data do not often follow a unique curve for the entire life of the reservoir which complicates the matching process resulting in unreliable prediction <sup>13</sup>. In their attempt at solving this problem, El-banbi *et al* <sup>13-16</sup>, came up with a Layered PSS Model that adequately captures the performance of gas wells, using a combination of MB ( $p/z$  Vs  $G_p$ ) and PSS equation. They suggested using the Ramaghost correction factor to account for water and rock compressibility and to linearize the  $p/z$  Vs  $G_p$  in a highly pressured gas reservoir. They applied their methods to tight gas and their results compared well with Simulation results. They obtained good match with field data provided transient data was not included in the analysis. They also applied this model to multiple layers and obtained good estimates for both *OGIP* and  $J_g$ . Ramaghost factor however employs constant rock compressibility which is not a good representation for unconsolidated rocks in deep water.

The methods described above either do not apply to multi-layered reservoir and / or do not include variable pore compressibility and its inherent effect on porosity, permeability and well productivity. They therefore can not correctly model the performance of wells in unconsolidated deep water formations.

Coupled Simulators<sup>17-18</sup> on the other hand combine Geomechanics calculations in a way that's too complex to be coded in a simple desktop application. Some authors including Settari<sup>19</sup> have suggested ways of approximating geomechanics equations and combining them with reservoir tools. An outline of developments in Geomechanics as applied to reservoir depletion is outlined below.

Several authors including Biot<sup>20-21</sup>, Geertsma<sup>22</sup> and Nur and Byerlee<sup>23</sup> related geomechanical stresses in porous medium (due to pressure depletion) to measured elastic moduli of solid rocks with applied external pressure as the latter are comparably easier to conduct in the laboratory. They demonstrated theoretically that for a homogenous isotropic porous medium undergoing an elastically linear deformation due to an external confining stress and an internal pore pressure, the effective stress law is given by Eq. 1.1 and the corresponding effective strain (change in bulk volume) is given by Eq. 1.2. For materials with negligible reservoir rock (or grain) compressibility with respect to the reservoir bulk compressibility, the value of the Biot's constant as given by Eq. 1.3 reduces to a value of one. Their work provided a relationship between measured pore compressibility in the laboratory due to applied external (compressive) stress to actual pore compressibility in the reservoir due to pressure depletion.

$$\sigma_e = \sigma_c + \alpha \sigma_p \quad 1.1$$

$$\varepsilon_f = \varepsilon_c - \alpha \varepsilon_p \quad 1.2$$

$$\alpha = 1 - \frac{c_r}{c_{bc}} \quad 1.3$$

Teeuw<sup>24</sup> and Mattax *et al*<sup>25</sup> compared different laboratory measurements of rock compressibility. Teeuw<sup>24</sup> provided a uniaxial correction factor (Eq. 1.4) to convert hydrostatic-test measurement of rock compressibility to reservoir condition by accounting for reservoir boundary effects of no lateral displacement. This uni-axial correction factor depends on rock's *Poisson* ratio. Practical values for reservoir rock *Poisson* ratio were provided by Holditch *et al*<sup>26</sup> for different hydrocarbon bearing formations using a correlation with log data.

$$c_{\phi m} = \frac{1}{3} \left( \frac{1+\nu}{1-\nu} \right) \alpha c_{\phi} \quad 1.4$$

Using hydrostatic test procedure and applying the uni-axial compressibility factor, Yale *et al*<sup>1</sup> measured variable rock compressibility using core samples from consolidated, friable and unconsolidated formations. They developed a seven-parameter variable rock compressibility correlation for consolidated, friable and unconsolidated formations (Eq. 1.5) given the initial reservoir pressure and the reservoir depth. The

parameters for each rock type are provided in Table 1.1. A typical plot of formation compressibility for each rock type using Yale's correlation is shown in Fig. 1.1

$$c_{\phi n}^n = A \left( K_1 * \text{ovb} - K_2 p^n + K_3 p_i - p^n - B \right)^C + D \quad 1.5$$

Constants	Consolidated sands	Friable sands	Unconsolidated sands
K <sub>1</sub>	0.85	0.90	0.95
K <sub>2</sub>	0.80	0.90	0.95
K <sub>3</sub>	0.45	0.60	0.75
A	-2.399 * 10 <sup>-5</sup>	1.054 * 10 <sup>-4</sup>	-2.805 * 10 <sup>-5</sup>
B	300	500	300
C	0.06230	-0.2250	0.1395
D	4.308 * 10 <sup>-5</sup>	-1.103 * 10 <sup>-5</sup>	1.183 * 10 <sup>-4</sup>

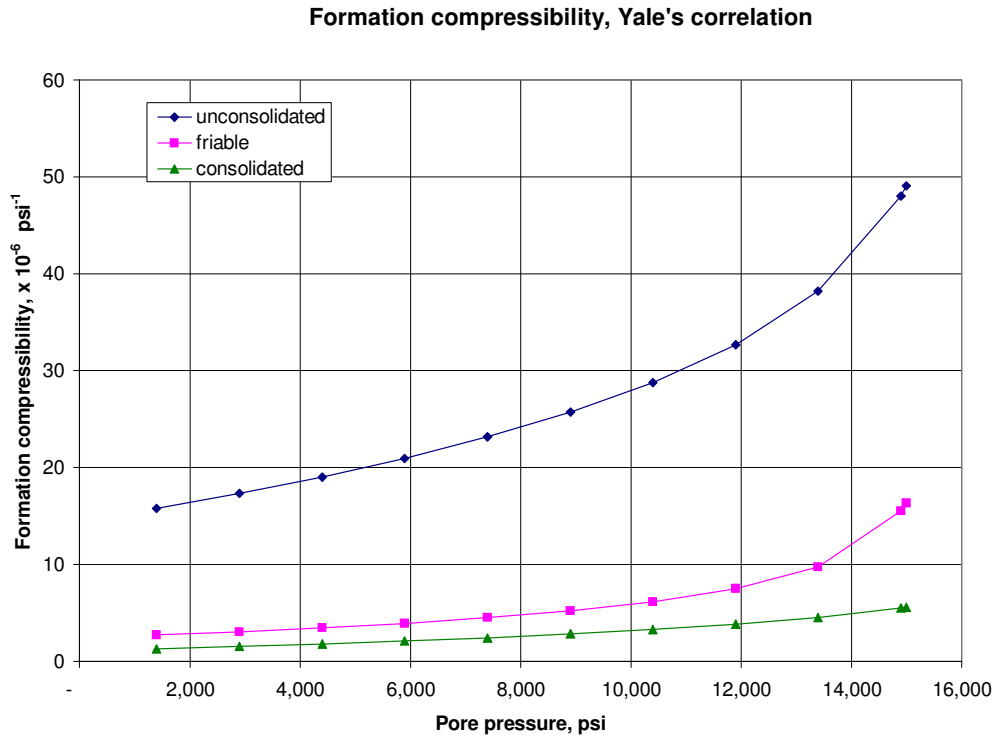


Figure 1.1: Formation compressibility using Yale's correlation

Ostermeier<sup>4-5</sup> performed similar experiments on cores samples from Deep water Gulf of Mexico unconsolidated sands and measured the porosity and permeability reductions due to external applied pressure on different types of rocks. He related this to changes due to reservoir pressure depletion. From his work the value of permeability to porosity ratio ( $m$ ), as described by Eq. 1.6, varied between 5 and 6.

$$\frac{k}{k_i} = \left( \frac{\phi}{\phi_i} \right)^m$$

1.6

Since formation compressibility is unique for each rock type, by developing a set of equations using Yale's correlation, a more general Compartmentalized model that applies to all rock types can be developed. By also employing some of the Geomechanics calculations parameters such as reservoir compaction and permeability reduction which are relevant in producing from an unconsolidated reservoir could also be determined.

### 1.3 Objective and Procedure

The purpose of this research is to develop a Compartmentalized gas Depletion Model that applies not only to conventional consolidated reservoirs (with constant formation compressibility) but also to unconsolidated reservoirs (with variable formation compressibility) by including geomechanics, permeability deterioration and compartmentalization to estimate the *OGIP* and performance characteristics of each compartment in such reservoirs given production data. The model also gives an estimate of reservoir compaction with depletion pressure which can aid in selection of the right tubular that can withstand the accompanied stress thereby preventing casing or tubing collapse.

The approach is to use VBA and Microsoft Excel solver to solve a combination of geomechanics, material balance and pseudo-steady state equations. In the absence of laboratory measurement of reservoir rock properties, available correlation in the industry for important properties such as variable rock compressibility and Poisson ratio are used. Available industry correlations were also employed for gas properties.

Using the correlation developed by Yale *et al*<sup>1</sup> for both constant and variable pore compressibility the geomechanics aspect of the model estimates pore volume and permeability variation for each production time. This is then coupled with a multi-layered gas depletion model that estimates well performance using gas material balance equation and pseudo-steady state equation. This approach is similar to that used by El-banbi and Wattenbarger<sup>13</sup>. Theirs was however for a constant formation compressibility case.

The model is used to analyze synthetic production data to estimate the *OGIP* and  $J_g$  of each compartment in a compartmentalized gas reservoir. The analysis is done by history-matching gas rate with the model using synthetic cases developed with a commercial simulator. An optimization routine is defined on the error function between the model and the simulator values using Microsoft excel solver.

## II. COMPARTMENTALIZED DEPLETION MODEL

### 2.1 Gas Depletion Calculations

The general form of the diffusivity equation for a slightly compressible fluid is given by Eq. 2.1<sup>28</sup>

$$\nabla^2 p = \frac{\phi \mu c_t}{k} \frac{\partial p}{\partial t} \quad 2.1$$

Where

$$c_t = S_o c_o + S_w c_w + S_g c_g + c_\phi \quad 2.2$$

For gas flow, viscosity and gas compressibility coefficient are dependent on pressure resulting in a non linear form of Eq. 2.1. In order to linearize the gas diffusivity equation, Al-Hussainy *et al*<sup>27</sup> suggested the use of a pseudo pressure defined by Eq. 2.3 which transforms the gas diffusivity equation into a form (Eq. 2.4) with comparable solutions to those derived for slightly compressible fluid.

$$m(p) = 2 \int_0^p \frac{p}{\mu z} dp \quad 2.3$$

$$\nabla^2 m(p) = \frac{\phi \mu c_t}{k} \frac{\partial m(p)}{\partial t} \quad 2.4$$

During pseudo-steady state conditions of closed outer boundary and constant pressure inner boundary, the solution to the gas diffusivity equation can be represented by the form given by Eq. 2.5 <sup>29</sup>.

$$q_g = \frac{k h [m(\bar{p}) - m(p_{wf})]}{1424 T \left[ \ln \frac{r_d}{r_w} + s + D_q q_g \right]} \quad 2.5$$

Where D is the non-Darcy coefficient and  $r_d$  is defined by Eq. 2.6 for circular reservoirs and by Eq. 2.7 for irregular reservoirs. For circular reservoir with one well in the middle, the time to attain *PSS* condition from transient flow is given by Eq. 2.8. If non Darcy coefficient is ignored and skin factor is constant, the real gas flow during *PSS* can be represented by the simple form in Eq. 2.9.

$$r_d = 0.472 r_e \quad 2.6$$

$$r_d = \frac{r_w}{2} \sqrt{\frac{10.06 \text{ Area}}{C_A r_w^2}} \quad 2.7$$

$$t_{pss} = 15.8 \frac{\phi \mu c_t \text{ Area}}{k} \quad 2.8$$

$$q_g = J_g [m(\bar{p}) - m(p_{wf})] \quad 2.9$$

where

$$J_g = \frac{1.987 * 10^{-5} k h \left( \frac{T_{sc}}{p_{sc} T} \right)}{\left[ \ln \frac{r_d}{r_w} + s + D_g q_g \right]}$$

Also the average reservoir pressure at any time during PSS can be estimated from material balance (M. B.) calculations using Eq. 2.11<sup>2</sup>.

$$p_i - \bar{p} = \frac{\Delta V}{c_t V} = \frac{q_g B_g}{c_t (\pi r_e^2 h \phi)} \quad 2.11$$

## 2.2 Model's Notation

- Compartments: In the model, each compartment is identified by the variable  $i_{res}$  and the total number of compartments by  $n_{res}$ .
- OGIP: The OGIP for each compartment is by  $OGIP_{ires}$ .
- Wells: Each well in the system is identified by the variable  $i_{well}$  and the total number of compartments by  $n_{well}$ .
- Productivity Indices: The productivity Index between each well-compartment system would be represented by a two-dimensional parameter  $J_g i_{well} i_{res}$ .

Using this nomenclature, a typical array of productivity indices in a four-compartment reservoir with five wells is shown below and indicates a total of ten completions.

Table 2.1 A typical array of productivity indices.

Reservoirs	OGIP <sub>1</sub>	OGIP <sub>2</sub>	OGIP <sub>3</sub>	OGIP <sub>4</sub>
Wells				
J <sub>g1</sub>	✓			
J <sub>g2</sub>			✓	✓
J <sub>g3</sub>				✓
J <sub>g4</sub>		✓	✓	✓
J <sub>g5</sub>	✓	✓	✓	

- Flux coefficient: The inter reservoir flow coefficient represents the flow between two compartments. A typical array of flux coefficients in a four-compartment reservoir is shown below and indicates a total of six distinguishable fluxes.

Table 2.2 A typical array of flux coefficients among different compartments.

Reservoirs	i <sub>res</sub> = 1	i <sub>res</sub> = 2	i <sub>res</sub> = 3	i <sub>res</sub> = 4
i <sub>res</sub> = 1				
i <sub>res</sub> = 2	✓			
i <sub>res</sub> = 3	✓	✓		
i <sub>res</sub> = 4	✓	✓	✓	

### 2.3 Models' Calculations for a Single Layer Case

A single layer depletion model describes the production performance of a single well completed in a single layered reservoir producing at a given  $p_{wf}$  as depicted in Fig.

2.1. The step by step calculations are described below.

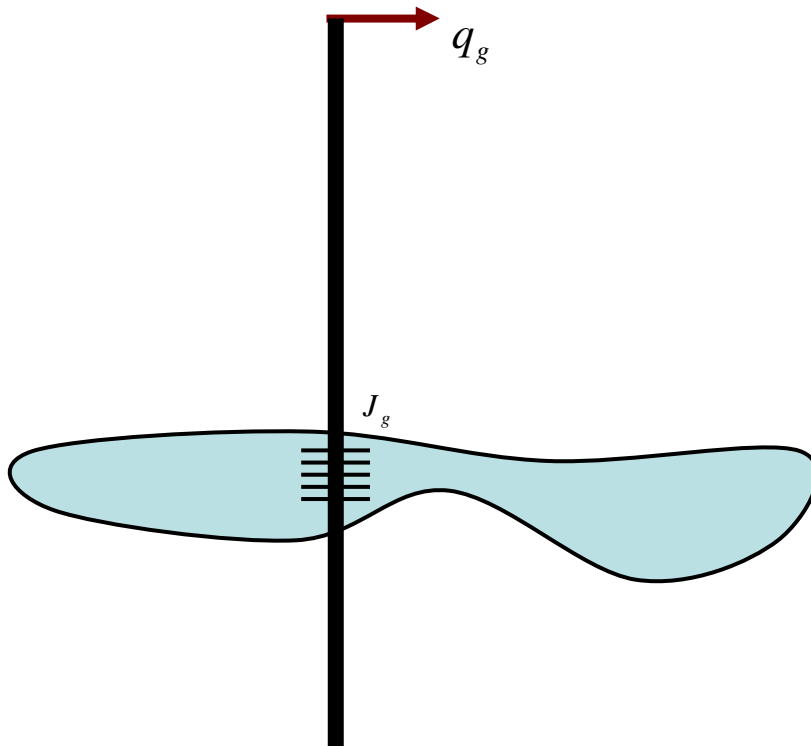


Figure 2.1: One layer Model

1. Based on input reservoir properties initial estimates of OGIP ( $OGIP_{guess}$ ) and Productivity Index ( $J_{g\_guess}$ ) provided by the user, the model calculates the following pressure dependent properties for each time step (Eqs. 2.12 – 2.17).

- Variable uniaxial pore volume compressibility ( $c_{\phi}^n$ ) using Yale's correlation.

$$c_{\phi}^n = A \left( K_1 * ovb - K_2 p^n + K_3 p_i - p^n - B \right)^C + D \quad 2.12$$

- Pore volume ( $V_p^n$ )

$$V_p^n = V_{p_i} e^{-c_{\phi m} (p_i - p^n)} \quad 2.13$$

$$\text{Where } V_{p_i} = \frac{OGIP_{-guess} B_{g_i}}{S_g} \quad 2.14$$

- Total compressibility ( $c_t^n$ )

$$c_t^n = c_{\phi m}^n + c_w S_w^n + c_g^n S_g^n \quad 2.15$$

- Pressure dependent productivity Index ( $i_{well} = i_{res} = 1$ )

$$J_g^n = J_{g\_guess} * \left( \frac{k^n}{k_i} \right) \quad 2.16$$

Where

$$\frac{k^n}{k_i} = \left( \frac{\phi}{\phi} \right)^m = \left[ e^{-c_{\phi m}^n (p_i - p^n)} \right]^m \quad 2.17$$

- Reservoir Compaction

$$\Delta h = \int_{p_i}^{p_{n_{time}}} h(p) * c_{bm}(p) dp \quad 2.18$$

or in finite difference form:

$$\Delta h = \sum_1^{n_{time}} h^n * c_{bm}^n * (p^{n-1} - p^n) \quad 2.18b$$

Where

$$c_{bm}^n = \phi * c_{\phi m}^n \quad 2.19$$

2. Solve simultaneously for gas rate and reservoir average pressure  $p_{\text{bar}}$  at the new time-step at pseudo-steady state condition (Eqs. 20 & 21).

$$q_g^{n+1} = J_g^n \left[ m(\bar{p}^{n+1}) - m(p_{wf}^{n+1}) \right] \quad 2.20$$

$$\bar{p}^{n+1} = \bar{p}^n - \frac{q_g^{n+1} B_g^n}{V_p^n c_t^n} \Delta t \quad 2.21$$

3. Compare calculated and measured gas rate for each time step, define an objective error function (Eq. 2.22) and minimize the normalized cumulative error thereby matching both measured rate and average reservoir pressure and estimating correct values for OGIP and  $J_g$ .

$$e_{r1} = \frac{1}{n_{time}} \sum_1^{n_{time}} \left| \text{Log } q_{g\_data} - \text{Log } q_{g\_model} \right| \quad 2.22$$

4. Once these two parameters (*OGIP and  $J_g$* ) are determined, the production-rate performance of the model is uniquely defined and production forecast for the well can be predicted. The historical and future compaction and productivity reduction profiles are also generated by the model.

## 2.4 Model's Calculations for a Multiple Layer Case

A multiple-layer depletion model describes the production performance of a single well completed in two or more reservoir layers as depicted in Fig. 2.2. These layers are commingled within the wellbore with the possibility of communication downhole. For a system of two layers, five parameters:  $OGIP_1$ ;  $OGIP_2$ ;  $J_{g1, 1}$ ;  $J_{g2, 1}$  and  $C_{1, 2}$  will uniquely describe the model where  $C$  represents the inter-compartment flow coefficient. Using a similar approach as described above for the single-layer case, these parameters can be estimated and the well forecast predicted.

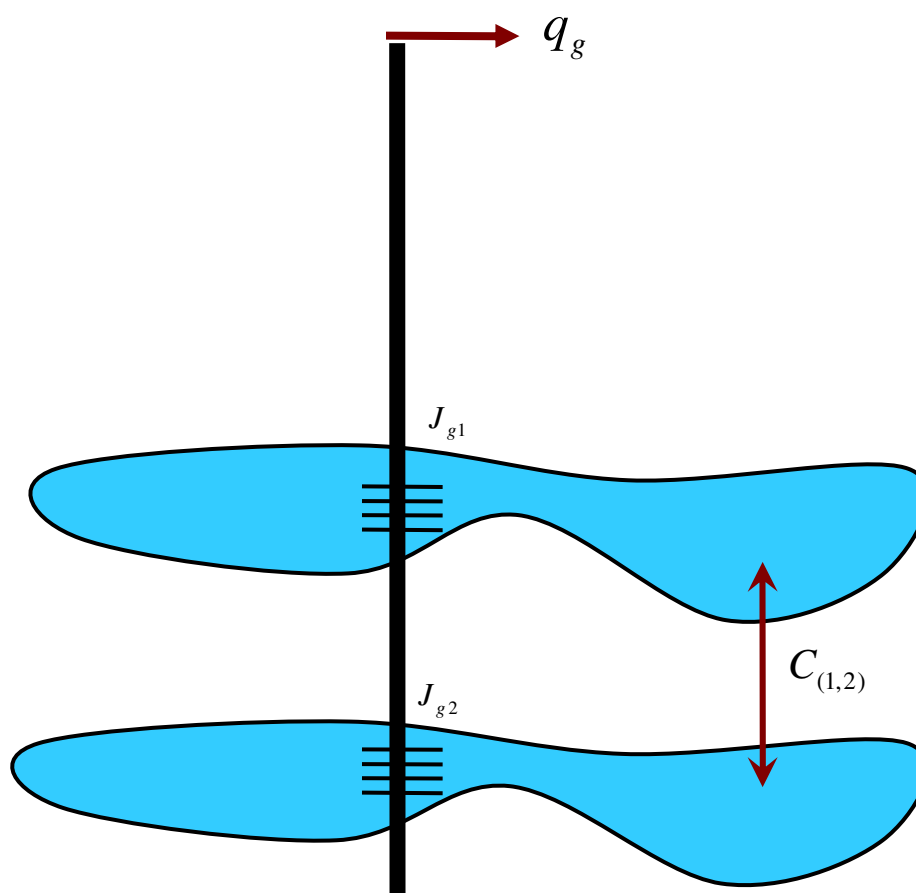


Figure 2.2: A typical 2-layer model with crossflow.

The *gas rate Vs Time* profile for each layer is calculated using the same set of equations as for one layer case in steps 1 and 2 above assuming the FBHP was equal for all layers and added to obtain total calculated rate for all layers.

The total calculated well rate is compared to the surface measured gas rate for each time step and using an objective error function (Eq. 2.23) an optimization routine minimizes the error difference matches  $q_g$  Vs *Time* and estimates a correct value for OGIP and Productivity Index for each layer.

$$e_{r2} = \frac{1}{n_{time}} \sum_1^{n_{time}} \left| \text{Log } q_{g\_data} - \sum_1^{n_{res}} \text{Log } q_{g\_model} \right| \quad 2.23$$

## 2.5 Model's Calculations for an entire field

This case captures actual arrangement in a field development in which each compartment could be drained by multiple wells and each well could be producing from more than one compartment. The different well-to-compartment interactions are therefore taken into consideration in describing the performance of each well and the entire field. The model also captures possible flow between different compartments within the reservoir. As with the single layer and multiple-layer models, the flow equation for each well-compartment system combines single phase gas flow with geomechanics by considering the effects of variable pore volume and pressure dependent permeability on gas productivity. In order to uniquely describe the system, the model expands the single layer calculations to determine the *OGIP* for all compartments, the productivity indices for each well-compartment system and the inter-compartment flux coefficients among different layers.

The *gas rate Vs Time* profile for each layer is calculated and summed up across the wells in the field in a manner similar to that for multiple layer case assuming same *FBHP* for each well. The total calculated well rate is compared to the field surface measured gas rate for each time step. The objective error function for this case is given by (Eq. 2.24).

$$e_{r3} = \frac{1}{n_{time}} \sum_1^{n_{time}} \left| \sum_1^{n_{well}} \text{Log } q_{g\_model} - \sum_1^{n_{well}} \sum_1^{n_{res}} \text{Log } q_{g\_data} \right| \quad 2.24$$

## 2.6 Data Input and Output

The input data for the model are categorized under reservoir, production and estimated data as follows:

- Reservoir data:

Initial reservoir pressure: (psi)

Reservoir depth (ft)

Connate water saturation

Water compressibility (1/psi)

Permeability-to-Porosity Relationship Exponent (m)

- Production data:

Daily / Monthly gas rate (scf/D)

Flowing bottom hole pressure (psi)

- Estimated Data:

A starting guess value for original gas in place:  $OGIP_{guess}$

A starting guess value for Initial Productivity Index:  $J_{g_{guess}}$

### Model Output:

Original Gas in Place for each layer: OGIP (MMscf)

Initial Productivity Index for each layer:  $J_{gi}$  (MMscf-cp/D/psi<sup>2</sup>)

Production profile for the reservoir

Reservoir Compaction

Permeability Reduction with time

## 2.7 Running the Model

Daily or monthly production data (excluding data in the transient flow regime) are supplied to the Compartmentalized Depletion Model, guess values for  $OGIP$  and  $J_g$  for each compartment are entered, and one of the three optimization criteria, namely: (i) changing  $OGIP$  only, (ii) changing  $J_g$  only or (iii) changing both  $OGIP$  and  $J_g$ , is selected. For reservoirs with more than one compartment, the user may have alternate among the three optimization criteria until reasonable estimates for  $OGIP$  and  $J_g$  are calculated by the model. The accuracy of model results can be evaluated using the residual (the cumulative difference in daily gas rate between the input data and the model) after each optimization. A cumulative residual of less than 1 MMscf generally gave comparable results to the Simulator. After a successful run, the model gives an estimate for  $OGIP$  and  $J_g$  for each layer. Once these parameters are known the production profile of the reservoir can be predicted over the life of the well.

## 2.8 Model's Characteristics and Assumptions

### Characteristics of Depletion Models

- It requires surface production rate and flowing BHP as input parameters.
- It considers the effects of variable pore pressure compressibility, variable permeability and variable productivity index in estimating reservoir performance.
- The optimization routine is done with VBA using Excel solver.

### Model Assumptions

- The reservoir is in stabilized flow under pseudo-steady state conditions at constant pressure with no aquifer influx.
- Non-Darcy effect is neglected.
- Transient data is not considered.

### III. RESULTS WITH CONSOLIDATED RESERVOIRS

#### 3.1 Single Layer Conventional Consolidated Reservoir

Gas rate data were generated for different reservoir layers that differ only in permeability (Table 3.2). Other reservoir properties are presented in Table 3.1 while the formation compressibility is derived from Yale's correlation using the appropriate parameters for consolidated rock as given in Table 1.1. Assuming equal *FBHP* for each layer, several linear combinations of these layers are used to create multiple layer reservoir cases. For single or multiple layer cases involving layers B to E, all production data points were used since their transient periods are small, otherwise, data points past the transient period were employed. Results with single layer consolidated reservoirs are presented in this section.

Data Preparation: production rate data for each compartment were simulated using GASSIM (a two dimensional, finite difference gas Simulator developed by the Reservoir Consortium Group at Texas A&M University). The simulator was run in the radial mode ignoring non-Darcy flow.

Area	80	acres
Reservoir thickness	50	ft
Porosity	0.1	
Initial Reservoir Pressure	2,500	psi
Gas Gravity	0.6	
BHFP	500	psi
Reservoir Temperature	150	F
Formation Compressibility	$3 * 10^{-6}$	1/psi
Well radius	0.25	ft
Simulation Data		
Number of Gridblocks	20	
OGIP	2892	MMscf

Compartments	Permeability (md)	$J_g$ (Mscf.cp/D/psi <sup>2</sup> )	$t_{pss}$ (days)
A	1	$7.59 * 10^{-6}$	38.8
B	10	$7.59 * 10^{-5}$	3.9
C	20	$1.52 * 10^{-4}$	1.9
D	50	$3.79 * 10^{-4}$	0.8
E	100	$7.59 * 10^{-4}$	0.4

Results for three cases (A, B, D) are shown to illustrate how the model calculates *OGIP* and Productivity Index for one-compartment cases. In each case, arbitrary guesses were made for both *OGIP* and Productivity Index before running the model. The model was run to match both gas rate.

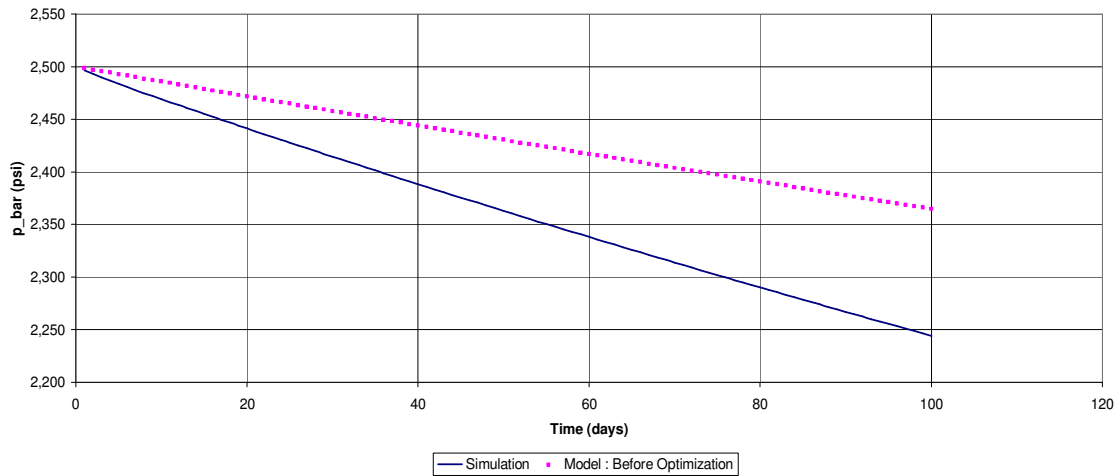
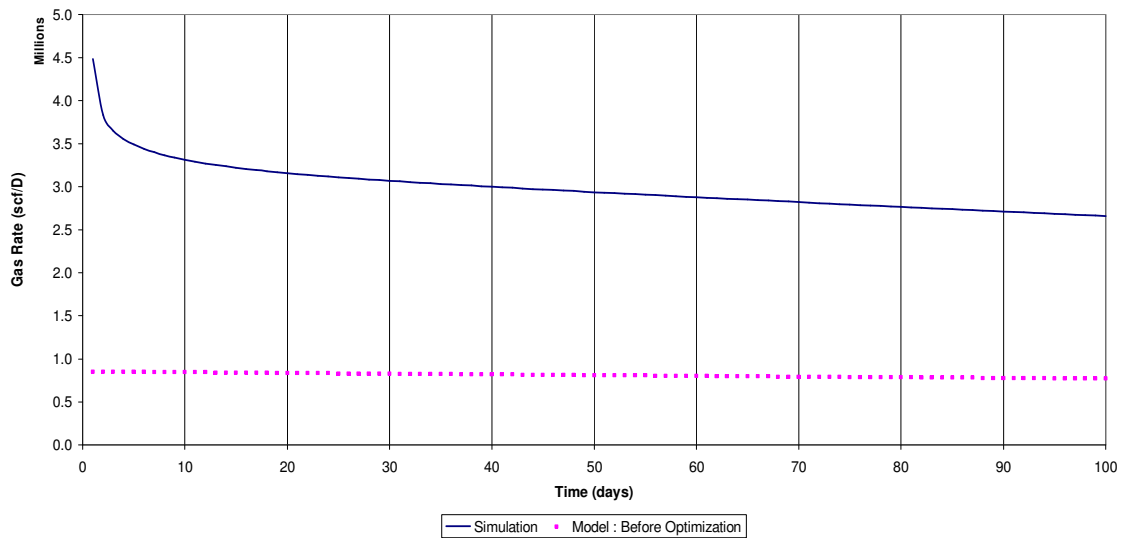
Case A: For Layer A with a formation permeability of 1 md the Productivity Index is calculated from Eq. 2.10 while the transient flow regime period is calculated from Eq. 2.8 (values shown in Table 3.2). Using the reservoir properties for layer A, daily production data were generated from the Simulator and the transient data eliminated before supplying it to the model. Figs. 3.1 & 3.2 is an example of gas rate and average reservoir pressure profiles from both the Simulator and the model before optimization and indicates that the initial guess values ( $OGIP_{guess}$  and  $J_{g_{guess}}$ ) supplied were lower than actual values. Figs. 3.3 & 3.4 represent the gas rate and reservoir average pressure profiles after optimization. The results show an excellent match between model and Simulation data and a good estimate for both *OGIP* and  $J_g$  as shown in Table 3.3 with an error of less than 1% for both parameters. The discrepancy between Simulator data and matched model data (Figs. 3.3 & 3.4) at early time represents the difference between Transient flow regime calculations by the Simulator and pseudo steady state assumption from the onset by the model.

Case B and Case D: Reservoirs B and D have permeabilities of 10 md and 50 md. An excellent match was also obtained for these cases with very good estimate of both *OGIP*

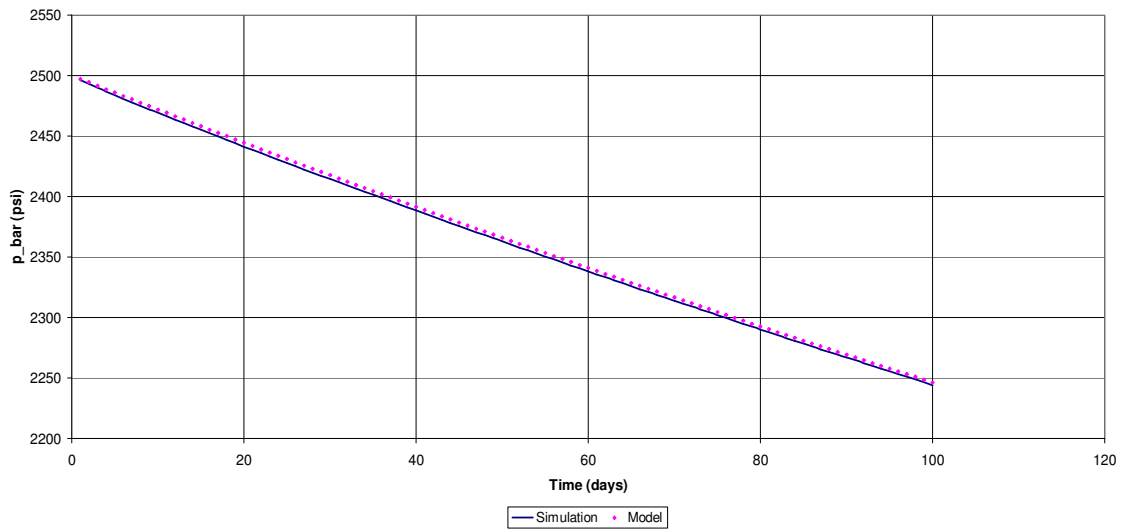
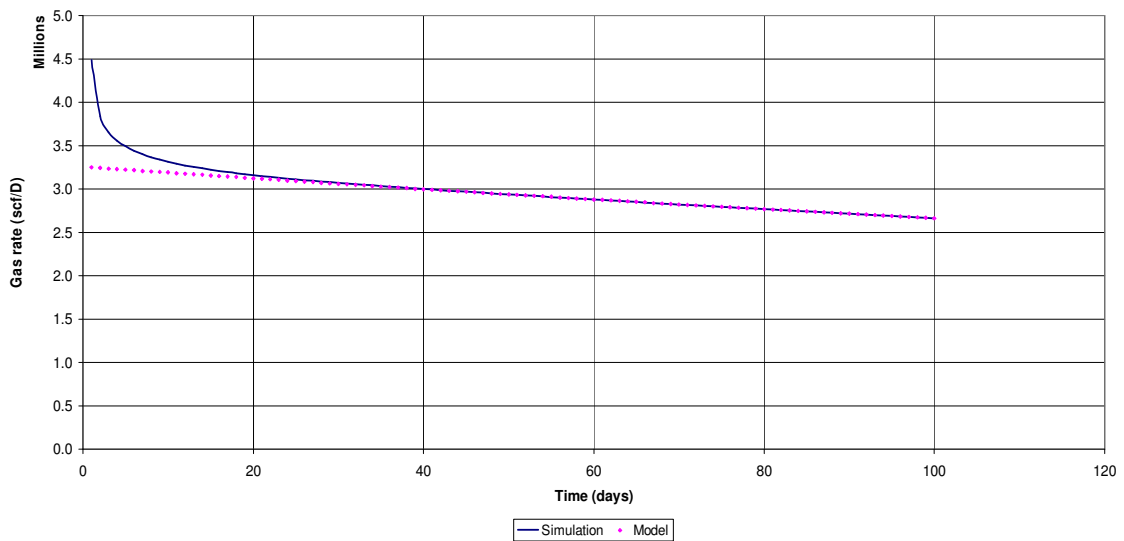
and  $J_g$  as shown in Figs. 3.5 – 3.8 and Tables 4 & 5. The percentage errors varied from 0.3% - 0.4% for OGIP and 1.5% to 6.6% for Productivity Indices.

**Effect of Including Transient Data in the Model:** In order to illustrate the effect of including transient production data in the model input, the model was re-run for Case A using all data from time zero. The results (Figs. 3.9 & 3.10, Table 3.3) show a less accurate estimate for both *OGIP* and  $J_g$  with the average percentage error increasing ten-fold.

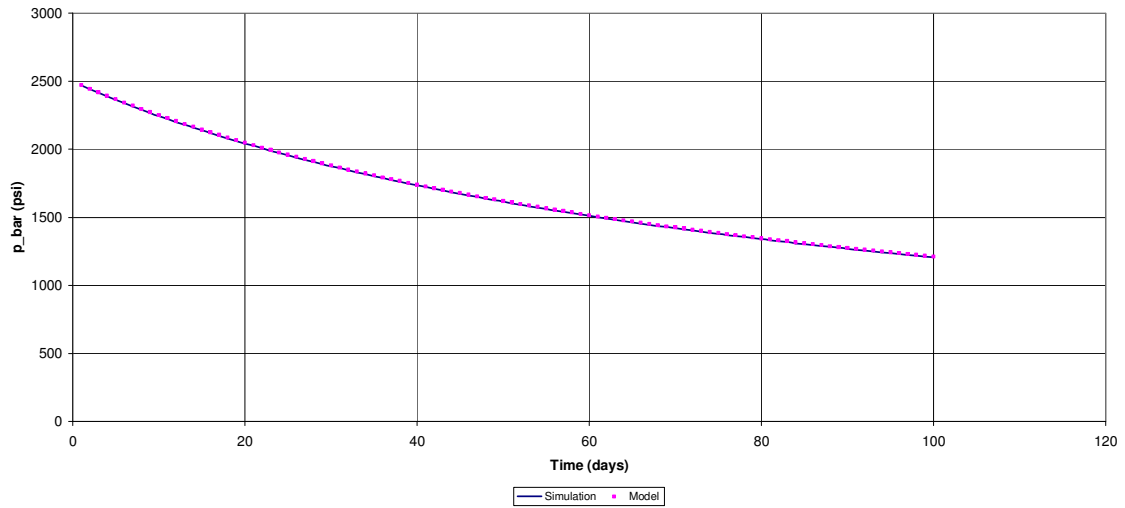
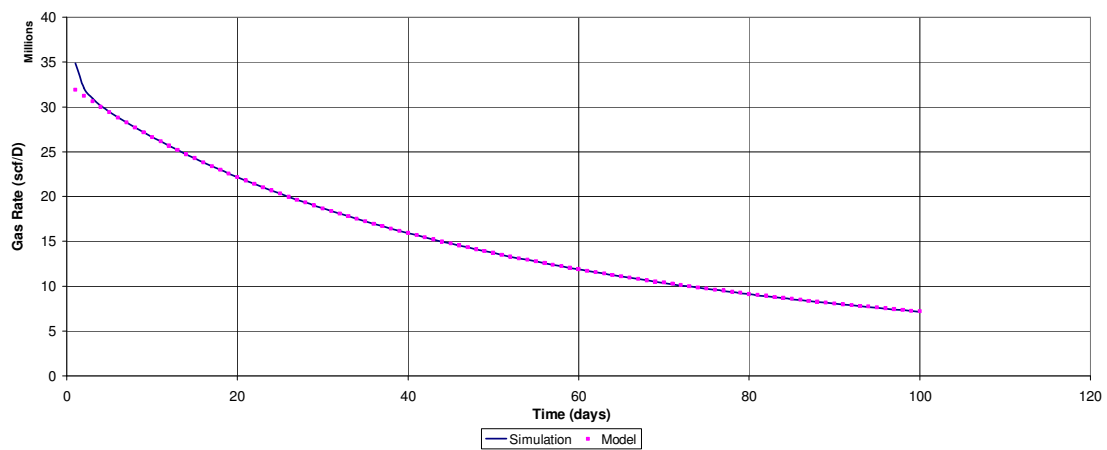
## 1-Layer Case A: Before Optimization

Fig. 3.1:  $p_{bar}$  Vs  $T$  for One Layer Case A, before OptimizationFig. 3.2:  $q_g$  Vs  $T$  for One Layer Case A, before Optimization

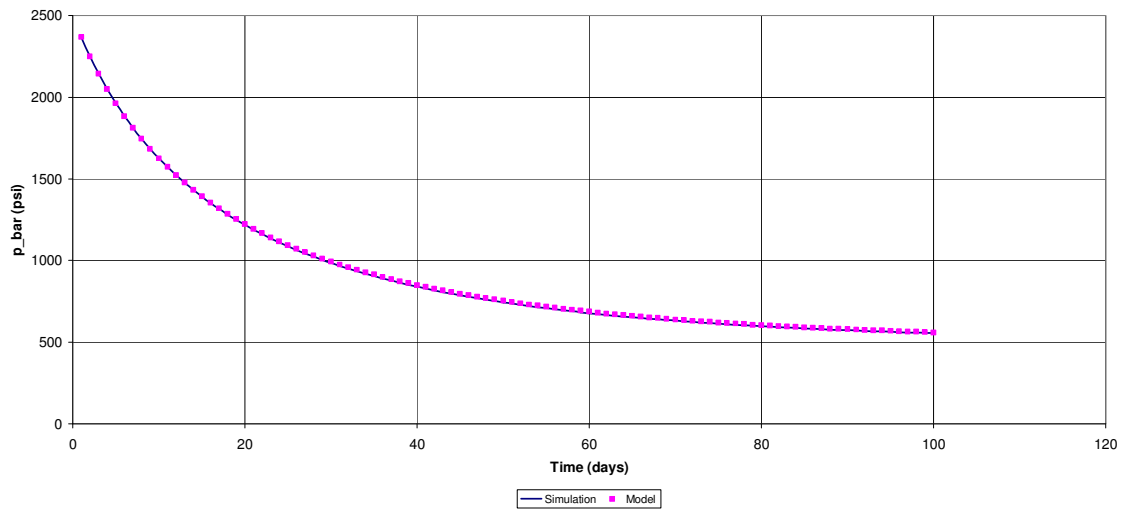
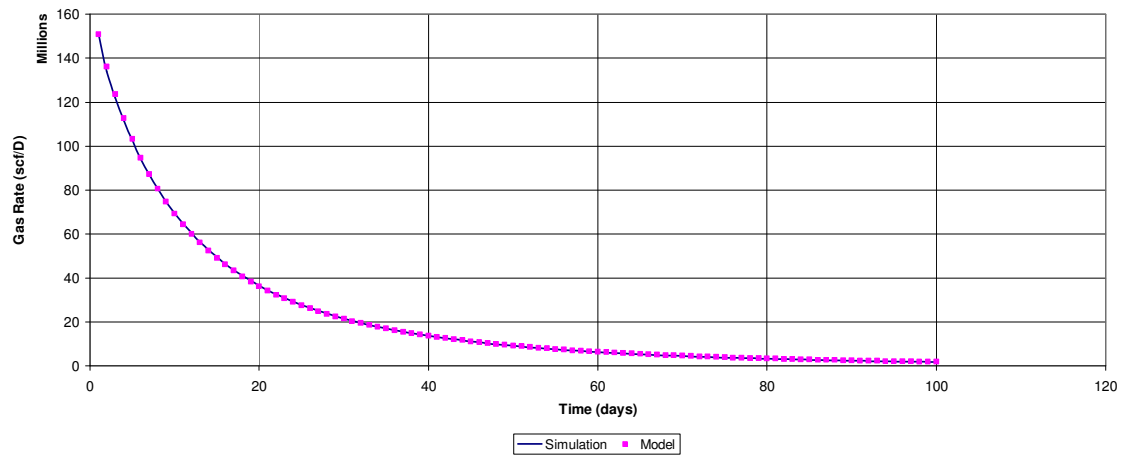
## 1-Layer Case A: after optimization

Fig 3.3:  $p_{bar}$  Vs  $T$  for One Layer Case A, after OptimizationFig. 3.4:  $q_g$  Vs  $T$  for One Layer Case A, after Optimization

## 1-Layer Case B

Fig. 3.5:  $p_{bar}$  Vs  $T$  for One Layer Case B, after OptimizationFig. 3.6:  $q_g$  Vs  $T$  for One Layer Case B, after Optimization

## 1-Layer Case D

Fig. 3.7:  $\bar{p}$  Vs  $T$  for One Layer Case D, after OptimizationFig. 3.8:  $q_g$  Vs  $T$  for One Layer Case D, after Optimization

### 1-Layer Case A: Including transient data

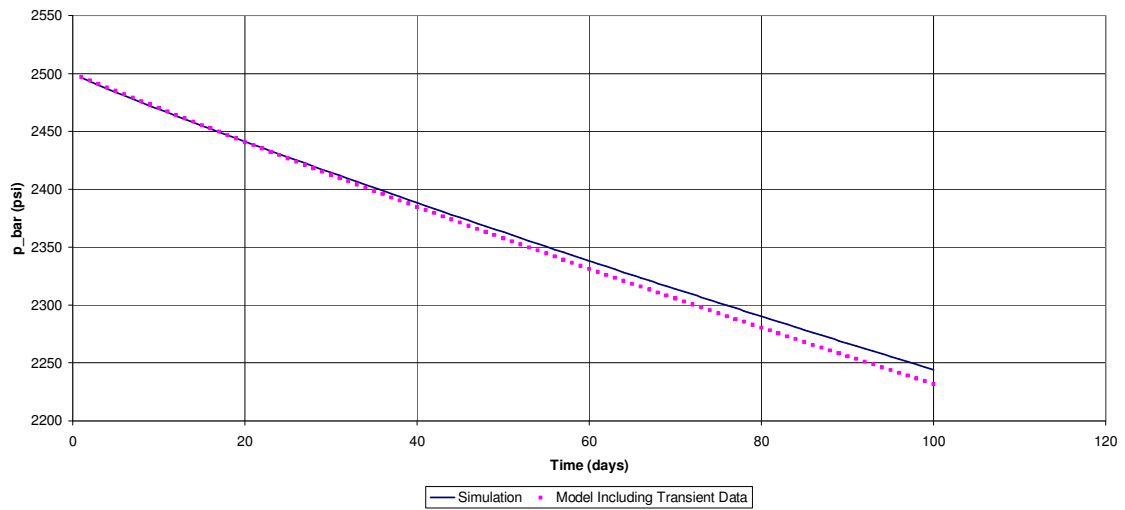


Fig. 3.9:  $\bar{p}$  Vs  $T$  for One Layer Case A, Including Transient data in Optimization

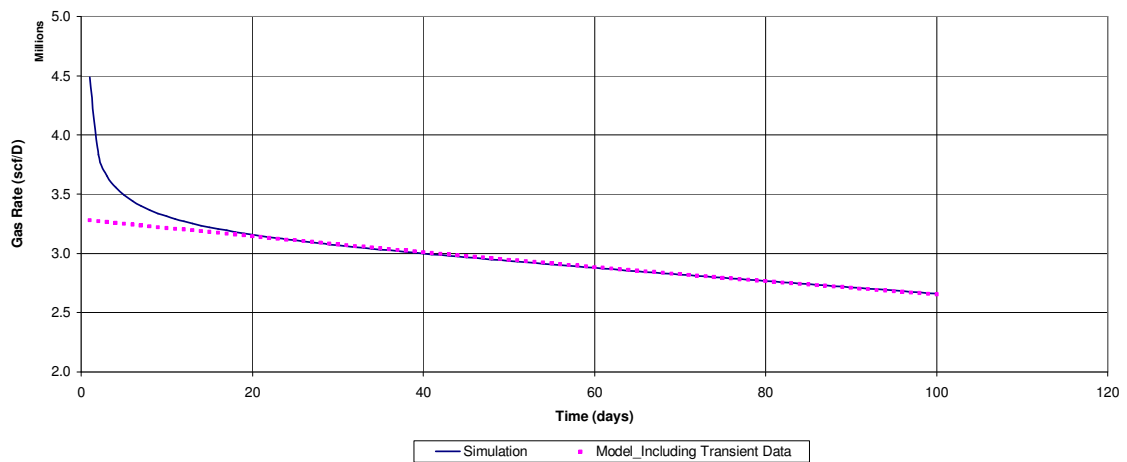


Fig. 3.10:  $q_g$  Vs  $T$  for One Layer Case A, Including Transient data in Optimization

## Results for One Layer Case with Consolidated Reservoir

Table 3.3: Results for Case A (k = 1 md)

	Simulator	Model	Error (%)	Model (including Transient data)	Error (%)
OGIP (MMscf)	2892	2887	0.2	2736	5.4
$J_g(\text{Mscf.cp/D/psi}^2)*10^{-6}$	7.59	7.63	0.5	7.70	1.3

Table 3.4: Results for Case B (k = 10 md)

	Simulator	Model	Error (%)
OGIP (MMscf)	2892	2904	0.4
$J_g(\text{Mscf.cp/D/psi}^2)$	$7.59 * 10^{-5}$	$7.49 * 10^{-5}$	1.5

Table 3.5: Results for Case D (k = 50 md)

	Simulator	Model	Error (%)
OGIP (MMscf)	2892	2884	0.3
$J_g(\text{Mscf.cp/D/psi}^2)$	$3.79 * 10^{-5}$	$3.54 * 10^{-5}$	6.6

### 3.2 Multi-Layer Conventional Consolidated Reservoir

For multiple layer cases, reservoir properties were taken from Table 3.1 while the production data for different compartments given in Table 3.2 were added to simulate two, three, four and five compartment systems flowing with the same FBHP. For all multiple compartment cases considered, the reservoirs were only combined in the wellbore with no communication in the formation.

#### Two- Layer Case

In the 2-layer case, a single well is completed both in layers C and D. Single layer simulated production data from GASSIM for layers C and D were added and inputted into the Model. Fig. 3.11 depicts the production profiles after optimization. Different combination of initial guesses was used. The model gave comparable results (see Table 3.6) for *OGIP* and  $J_g$  for each layer, though less accurate than the results obtained in the one-layer cases. For instance while the maximum error for the one-layer cases were 7%, the maximum error for the two-layer case increased to 11%.

#### Three-Layer Example (B-C-D)

In this 3-layer case, a single well is completed in layers B, C and D. As with the 2-layer case, simulator runs for layers A, B, C were added and inputted into the Depletion Model. The model was run systematically by alternating among the three optimizing criteria. The plots of  $q_g$  Vs  $T$  for simulator data and Model's calculations after the optimization are shown in Fig. 3.12 while the *OGIP* and Productivity Indices estimated

by the model in comparison with Simulator values are shown in Table 3.7. As expected, the estimates are less accurate than those provided with one or two layer cases but still less than 6% for *OGIP* and about 20% for productivity index.

#### Four-Layer and Five-Layer Cases

As with other cases, GASSIM runs for all the layers were added and inputted into the Depletion Model. The model was run systematically by alternating among the three optimizing criteria. The results (Fig. 3.13 & 3.14) show a fairly good match for both *OGIP* and  $J_g$  for each case. However, unlike cases with three layers and below where the model converged to good values irrespective of initial estimates, obtaining good results with four and five layer cases was dependent on initial estimates. In other words, good initial estimates were required before convergence.

## 2-Layer Case C-D

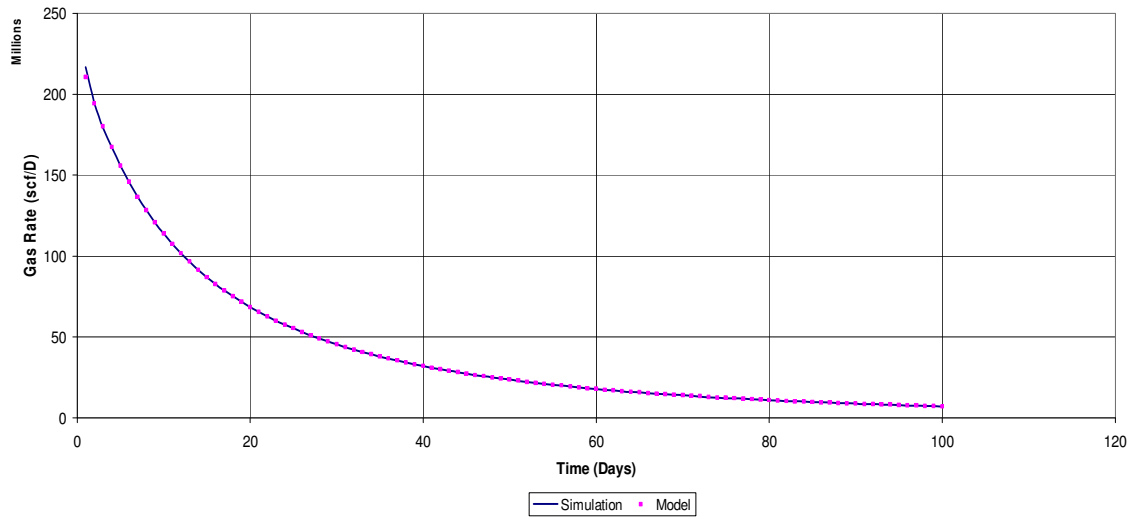
Fig. 3.11:  $q_g$  Vs  $T$  for 2-Layer Case C-D, after Optimization

Table 3.6: Results for two layer case C-D

	OGIP (MMscf)			$J_g$ (Mscf.cp/D/psi <sup>2</sup> ) *10 <sup>-4</sup>		
	Simulator	Model	Error (%)	Simulator	Model	Error (%)
C	2892	2882	0.4	1.52	1.57	3.4
D	2892	2843	1.7	3.79	3.38	11

## 3-Layer Case B-C-D

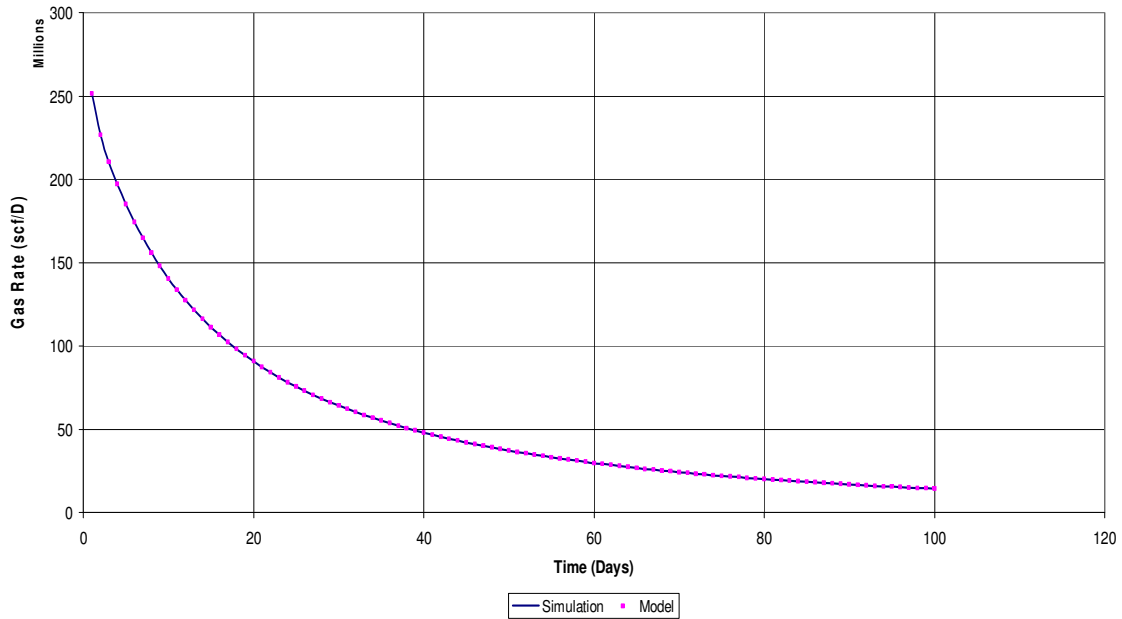
Fig. 3.12:  $q_g$  Vs  $T$  for 3-Layer Case B-C-D, after Optimization

Table 3.7: Results for three layer case (B-C-D)

	OGIP (MMscf)			$J_g$ (Mscf.cp/D/psi <sup>2</sup> )*10 <sup>-5</sup>		
	Simulator	Model	Error (%)	Simulator	Model	Error (%)
B	2892	2885	0.2	$7.59 * 10^{-5}$	$6.79 * 10^{-5}$	13.3
C	2892	2740	5.3	$1.52 * 10^{-4}$	$1.85 * 10^{-4}$	21.7
D	2892	3017	4.3	$3.79 * 10^{-4}$	$3.28 * 10^{-4}$	13.3

## 4-Layer Case A-B-C-D

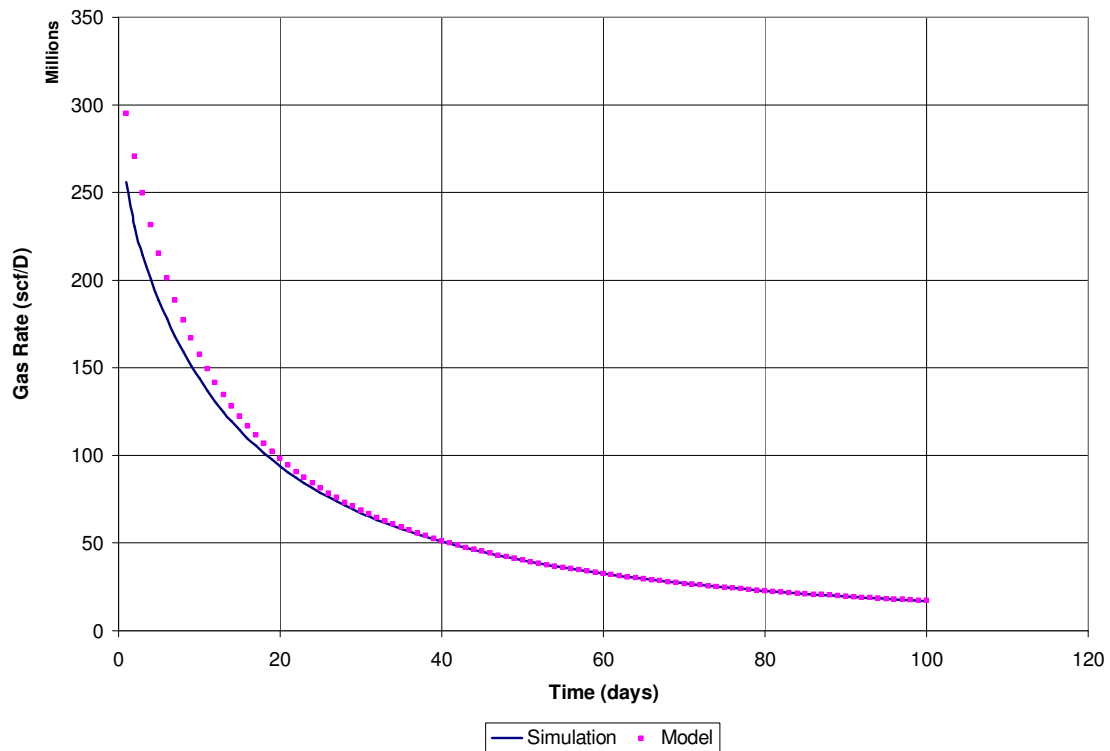
Fig. 3.13:  $q_g$  Vs  $T$  for 4-Layer Case A-B-C-D, after Optimization

Table 3.8: Results for four-layer case (A-B-C-D)

	OGIP (MMscf)			$J_g$ (scf.cp/D/psi <sup>2</sup> )		
	Simulator	Model	Error (%)	Simulator	Model	Error (%)
A	2892	3006	4.0	$7.59 * 10^{-6}$	$6.29 * 10^{-6}$	17.2
B	2892	2994	3.5	$7.59 * 10^{-5}$	$7.87 * 10^{-5}$	3.6
C	2892	2903	0.4	$1.52 * 10^{-4}$	$1.78 * 10^{-4}$	16.5
D	2892	2849	1.5	$3.79 * 10^{-4}$	$4.04 * 10^{-4}$	6.5

## 5-Layer Case A-B-C-D-E

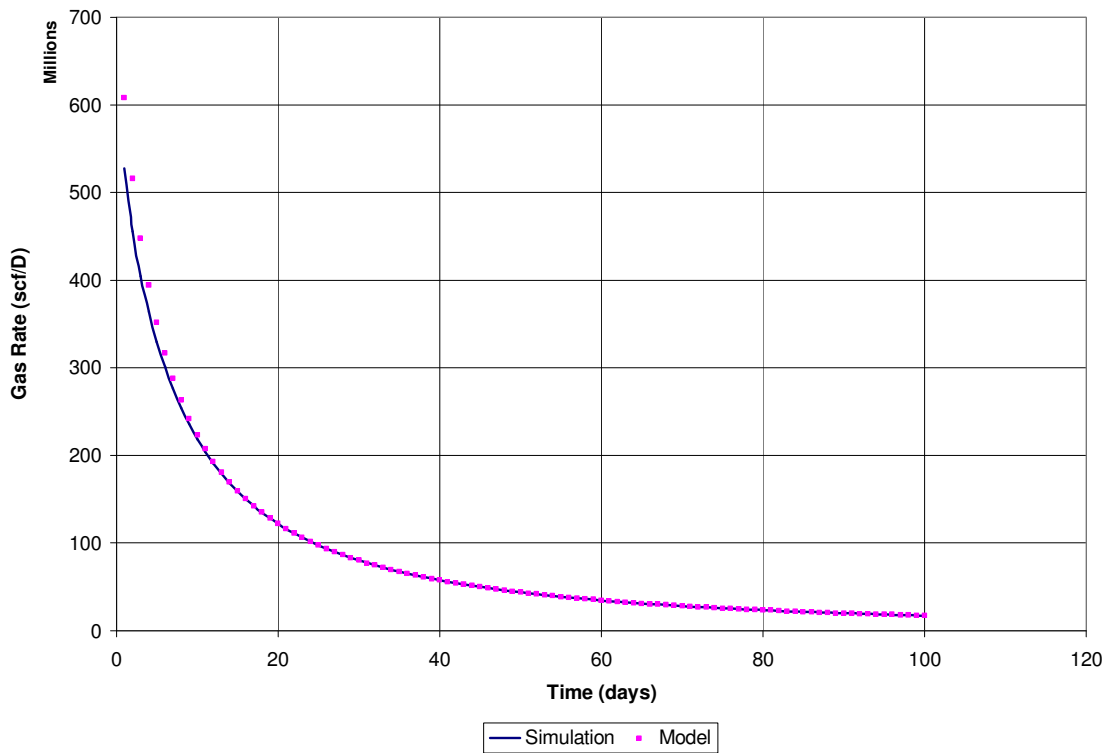
Fig. 3.14:  $q_g$  Vs  $T$  for 5-Layer Case A-B-C-D-E, after Optimization

Table 3.9: Results for five-layer case (A-B-C-D-E)

	OGIP (MMscf)			$J_g$ (scf.cp/D/psi <sup>2</sup> )		
	Simulator	Model	Error (%)	Simulator	Model	Error (%)
A	2892	3006	3.9	$7.59 * 10^{-6}$	$8.10 * 10^{-6}$	6.6
B	2892	3000	3.7	$7.59 * 10^{-5}$	$8.86 * 10^{-5}$	16.6
C	2892	2934	1.4	$1.52 * 10^{-4}$	$1.54 * 10^{-4}$	1.3
D	2892	2893	0.1	$3.79 * 10^{-4}$	$3.82 * 10^{-4}$	0.8
E	2892	2906	0.5	$7.59 * 10^{-4}$	$7.95 * 10^{-4}$	4.5

#### IV. RESULTS WITH UNCONSOLIDATED RESERVOIRS

##### 4.1 Application to Single Layer Deep water Unconsolidated Reservoirs

For unconsolidated reservoir, gas rate data were generated for different reservoir layers that differ in *OGIP*, permeability and pay thickness (Table 4.2). Formation compressibility correlation and average porosity for unconsolidated reservoirs were taken from Yale *et al*<sup>1</sup> as given in Table 4.1. As used in the cases shown, deep water reservoirs generally have a large pay thickness. In order to demonstrate the dependence of compaction on reservoir pay thickness, layers C and D were chosen to vary only in their pay thickness.

Data Preparation: As GASSIM is not currently programmed to work with variable formation compressibility and other Geomechanics calculations, synthetic production data were generated from the Compartmentalized Depletion Model using known values of *OGIP* and  $J_g$  for each reservoir layer. These were then used as input data and the model was run with initial estimates of *OGIP* and  $J_g$  (Table 4.2b) which differs from actual values.

Geomechanics Calculation: Geomechanical parameters were calculated by the model every time step. These parameters include variable formation compressibility, change in permeability, change in productivity index and the compaction of the reservoir due to pressure depletion using Eq. 2.12 – 2.19 as described in Chapter 2.

Table 4.1: Reservoir properties for unconsolidated reservoir		
Area	40	acres
Initial Reservoir Pressure	10,000	psi
Reservoir Depth	12,000	ft
BHFP	1,500	psi
Reservoir Temperature	200	F
Gas Specific Gravity	0.5	
Porosity	0.325	
Formation Compressibility	Using Yale's Correlation	1/psi

Table 4.2: Properties for different unconsolidated reservoir layers					
Compartments	k(md)	OGIP (MMscf)	h (ft)	$J_g$ (Mscf.cp/D/psi <sup>2</sup> )	$t_{pss}$ (days)
A	10	11,267	50	$7.35 * 10^{-5}$	2.5
B	15	16,900	75	$1.65 * 10^{-4}$	1.7
C	20	22,533	100	$2.94 * 10^{-4}$	1.3
D	20	112,665	500	$1.47 * 10^{-3}$	1.3

Table 4.2b: Guess Values used in Running the Model for Single or Multiple Layered Cases		
Compartments	OGIP (MMscf)	$J_g$ (Mscf.cp/D/psi <sup>2</sup> )
A	6,000	$1 * 10^{-4}$
B	8,000	$2 * 10^{-4}$
C	10,000	$4 * 10^{-4}$
D	30,000	$5 * 10^{-4}$

Results for three cases (A, C and D) are shown to illustrate how the model calculates *OGIP* and productivity index for unconsolidated one-compartment cases. In each case, arbitrary guesses were made for both *OGIP* and Productivity Index (Table 4.2b). The model was run to match gas rate. Results are shown in Figs. 4.1 – 4.12. A perfect match for both *OGIP* and  $J_g$  were obtained in each case (Table 4.3 – 4.5). The compactions for reservoirs A, C and D were approximately 3 ft, 6 ft and 31 ft respectively (Figs. 4.3, 4.7 and 4.11) which is proportional to their pay thickness over the production period. Figs. 4.4, 4.8, and 4.12 show permeability variation with time and indicate a reduction of more than 65% in permeability in each case.

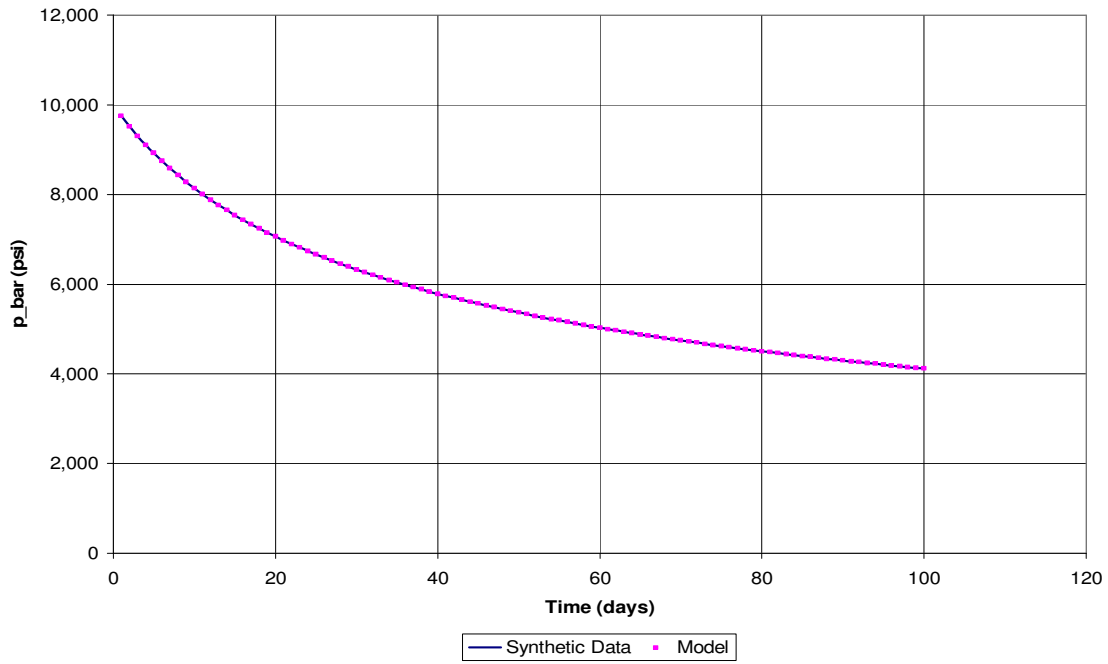


Fig. 4.1:  $p_{\text{bar}}$  Vs  $T$  for 1-Layer Case A, after Optimization

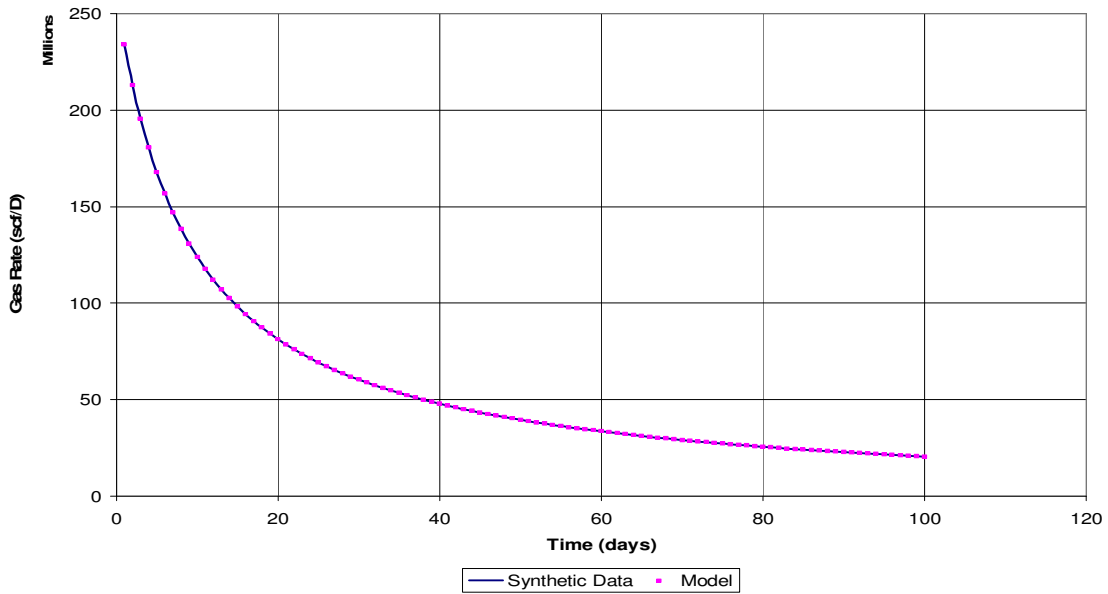


Fig. 4.2:  $q_g$  Vs  $T$  for 1-Layer Case A, after Optimization

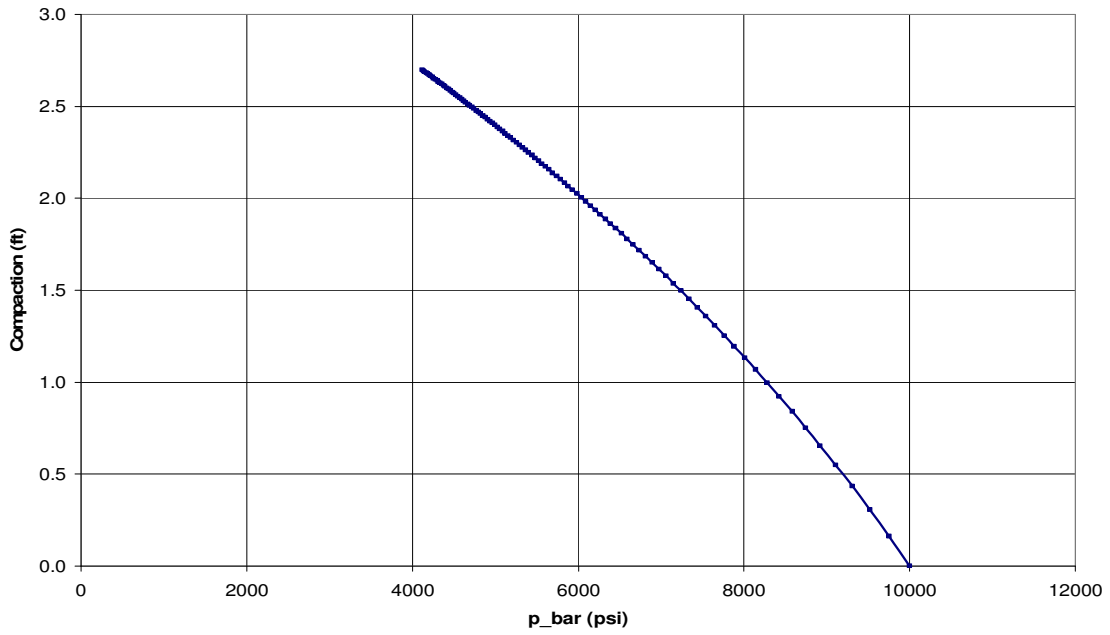


Fig. 4.3:  $dh$  Vs  $p_{bar}$  for 1-Layer Case A, after Optimization

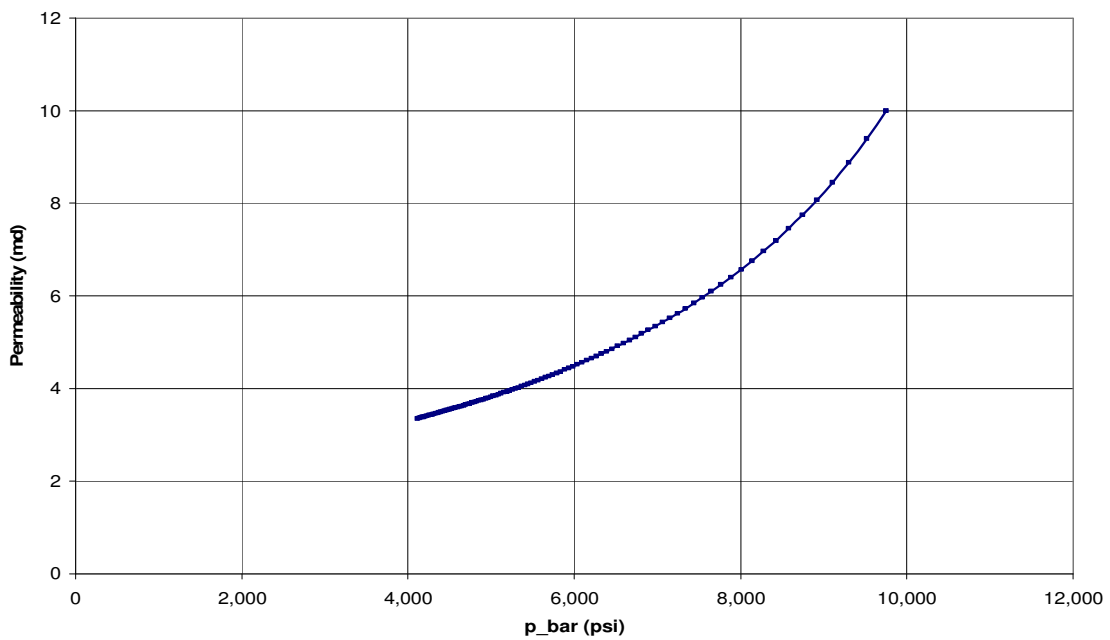


Fig. 4.4:  $k$  Vs  $p_{bar}$  for 1-Layer Case A, after Optimization

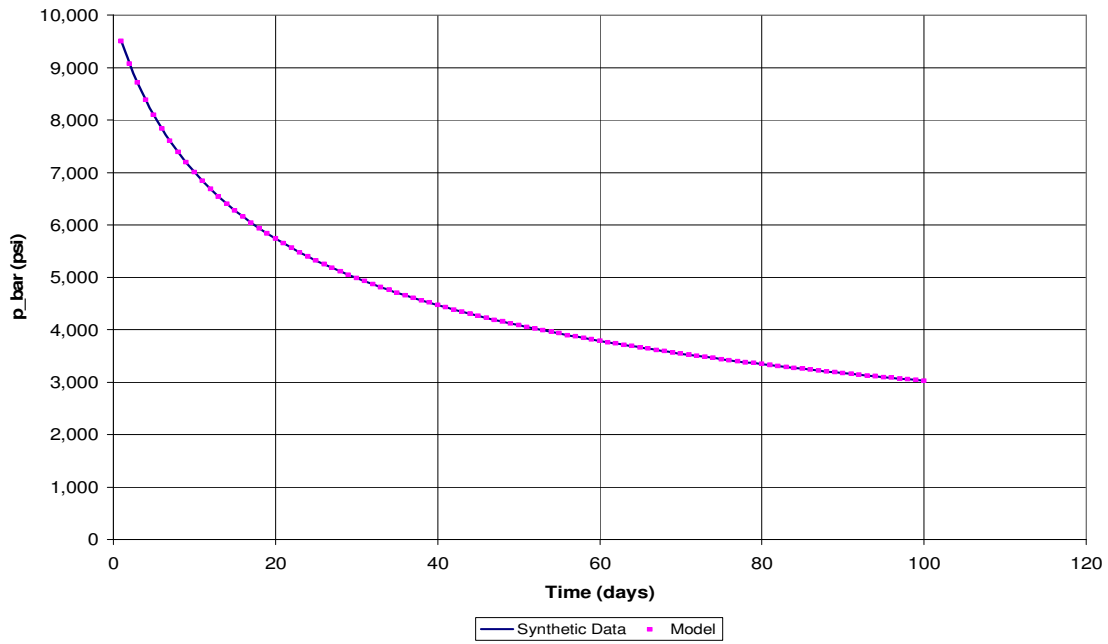


Fig. 4.5:  $p_{\text{bar}}$  Vs  $T$  for 1-Layer Case C, after Optimization

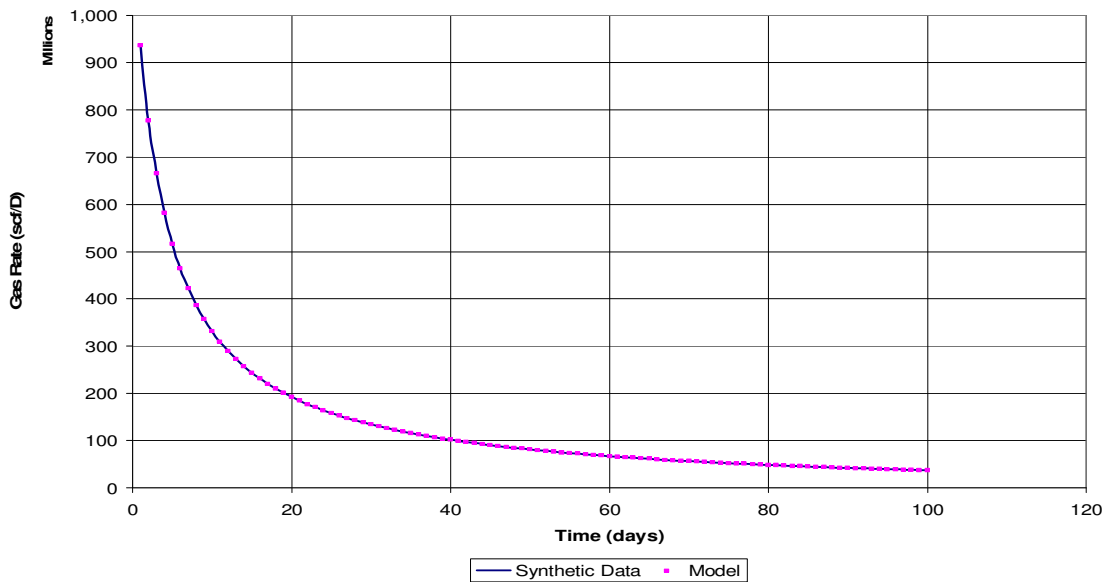


Fig. 4.6:  $qg$  Vs  $T$  for 1-Layer Case C, after Optimization

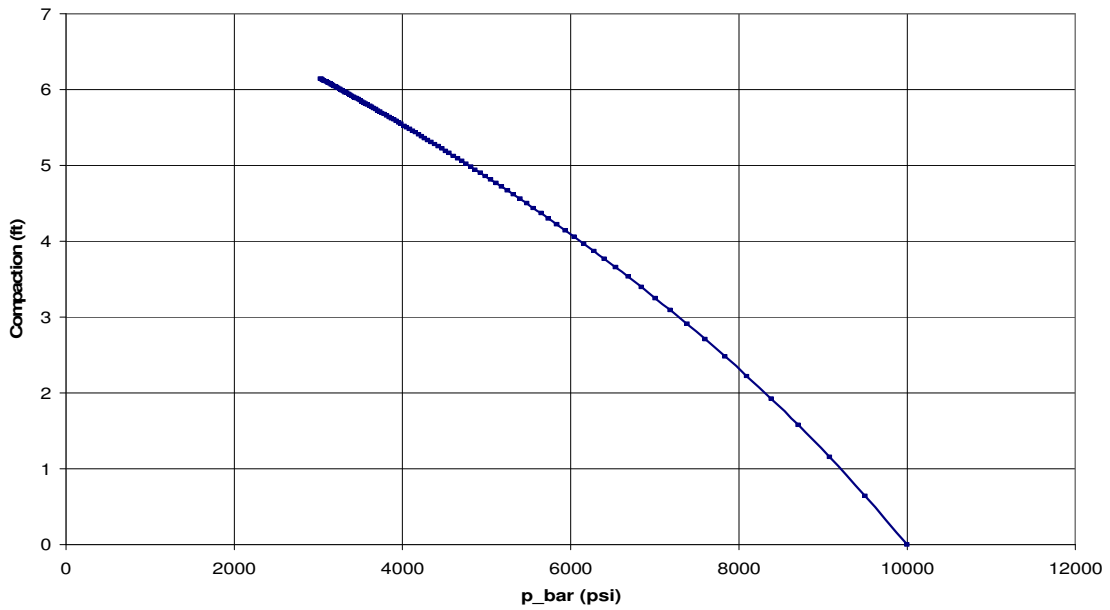


Fig. 4.7:  $dh$  Vs  $p_{bar}$  for 1-Layer Case C, after Optimization

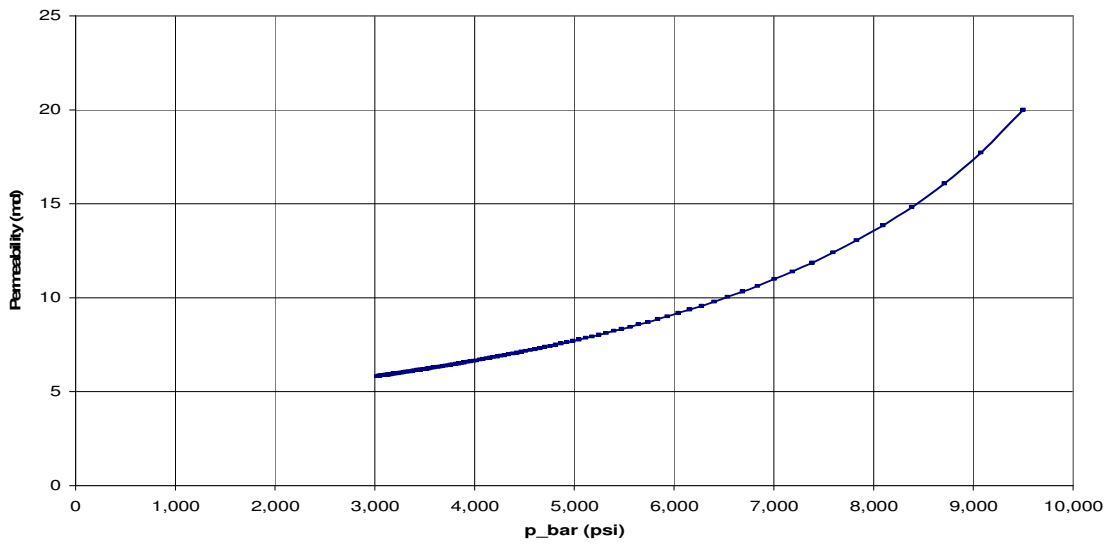


Fig. 4.8:  $k$  Vs  $p_{bar}$  for 1-Layer Case C, after Optimization

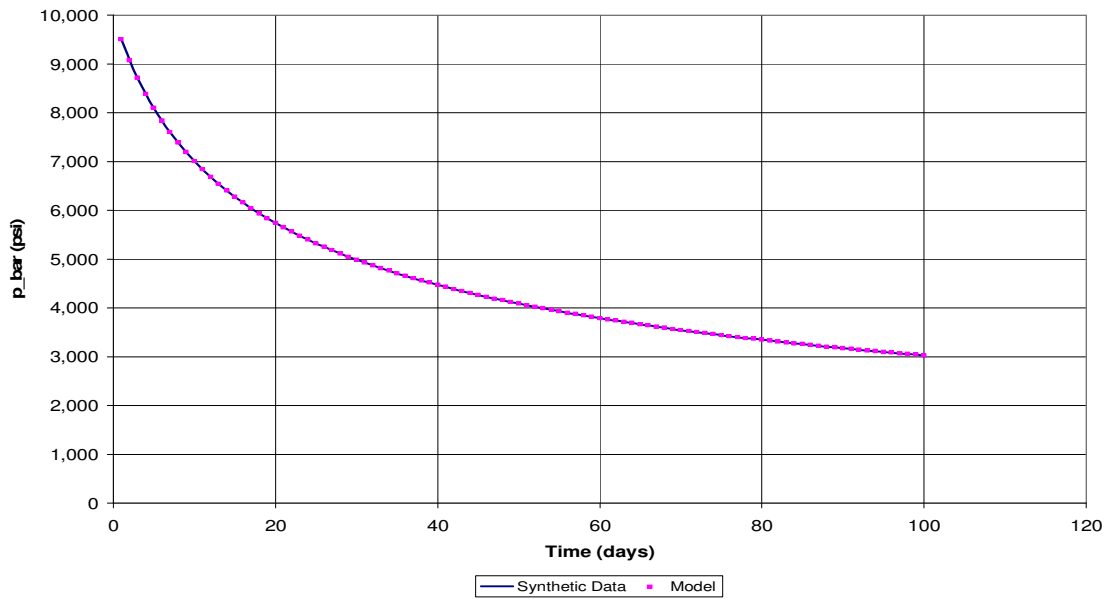


Fig. 4.9:  $\bar{p}$  Vs  $T$  for 1-Layer Case D, after Optimization

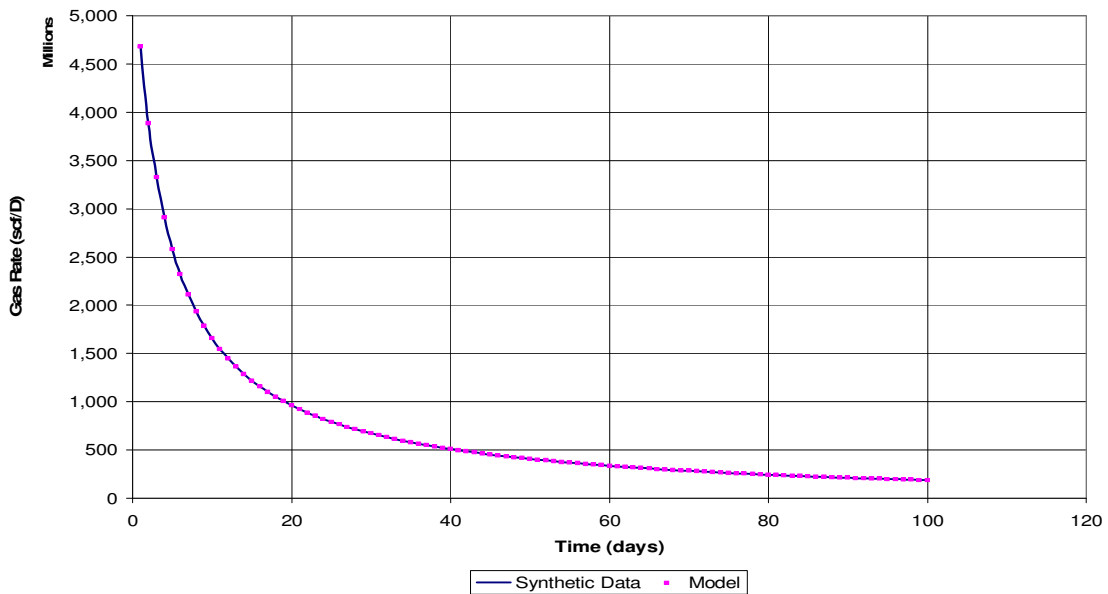


Fig. 4.10:  $q_g$  Vs  $T$  for 1-Layer Case D, after Optimization

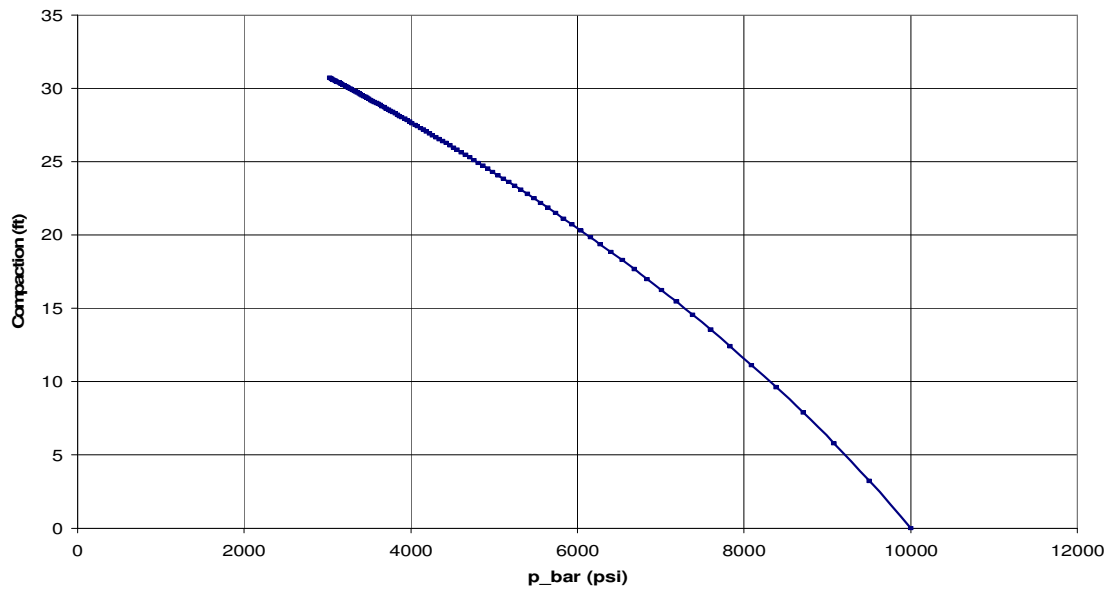


Fig. 4.11:  $dh$  Vs  $p_{bar}$  for 1-Layer Case D, after Optimization

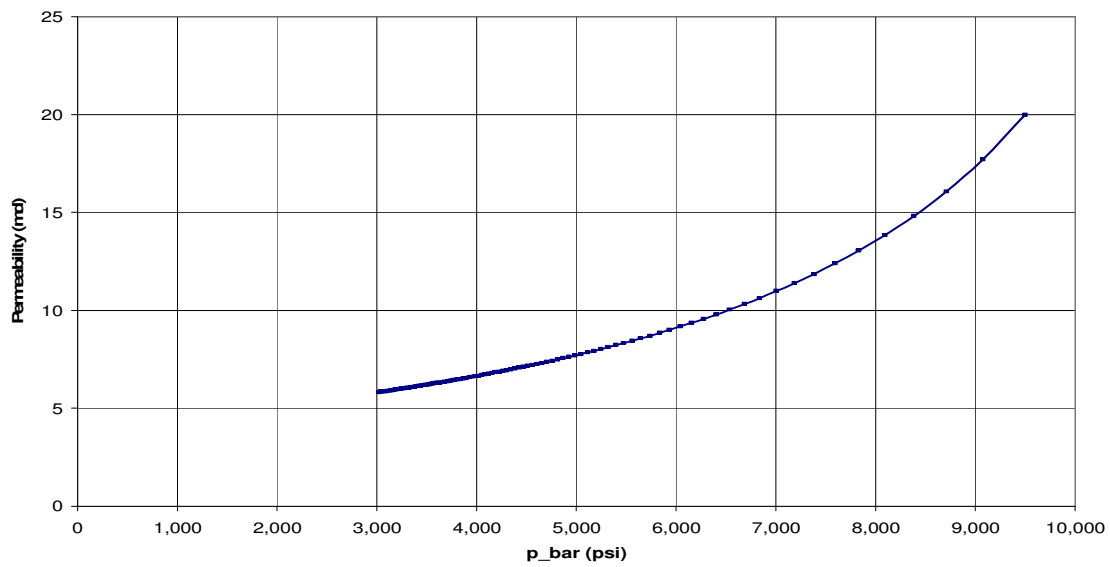


Fig. 4.12:  $k$  Vs  $p_{bar}$  for 1-Layer Case D, after Optimization

## Result for One-Layer Cases

Table 4.3: Results for 1-layer Case A (unconsolidated reservoir)				
	OGIP (MMscf)		$J_g$ (Mscf.cp/D/psi <sup>2</sup> )	
	Synthetic Data	Model	Synthetic Data	Model
A	11,267	11,267	$7.35 * 10^{-5}$	$7.35 * 10^{-5}$

Table 4.4: Results for 1-layer Case C (unconsolidated reservoir)				
	OGIP (MMscf)		$J_g$ (Mscf.cp/D/psi <sup>2</sup> )	
	Synthetic Data	Model	Synthetic Data	Model
C	22,533	22,533	$2.94 * 10^{-4}$	$2.94 * 10^{-4}$

Table 4.5: Results for 1-layer Case D (unconsolidated reservoir)				
	OGIP (MMscf)		$J_g$ (Mscf.cp/D/psi <sup>2</sup> )	
	Synthetic Data	Model	Synthetic Data	Model
D	112,665	112,665	$1.47 * 10^{-3}$	$1.47 * 10^{-3}$

## 4.2 Multi-Layer Unconsolidated Reservoir

For multiple layer cases, reservoir properties were taken from Table 4.1 while the production data for different compartments given in Table 4.2 were added to simulate multiple compartment systems flowing with the same *FBHP*. For all multiple compartment cases considered, the reservoirs were only combined in the wellbore with no communication in the formation.

### Two- Layer Cases

Two cases (A-B, A-C) were used to illustrate how the model calculates *OGIP* and  $J_g$  for two-compartment cases. Figs 4.13 & 4.16 show Daily Gas Rate profiles after running the optimization. The results for model's *OGIP* and  $J_g$  for each layer for cases A-B and A-C as compared to actual data are shown Tables 4.6 & 4.7. A fairly good match for both *OGIP* and  $J_g$  was obtained in each case. In either case, the percentage error varied from 0.5% – 2.3% for *OGIP* and 0.4% - 2.9% for Productivity Indices. There was however a perfect match for the combined *OGIP* and combined  $J_g$  in both cases. The net compaction over the given period was 7 and 9 ft respectively (Figs. 4.14 & 4.17).

### Three- Layer Case

Result for one three-layer case (A-B-C) is shown. The results for model's *OGIP* and  $J_g$  for each layer are less accurate but still comparable to actual data as shown Table 4.8. As with previous cases, there was still a perfect match for the combined *OGIP* and combined  $J_g$ . The net compaction for this case was 13 ft.

## 2- Layer Case (A-B)

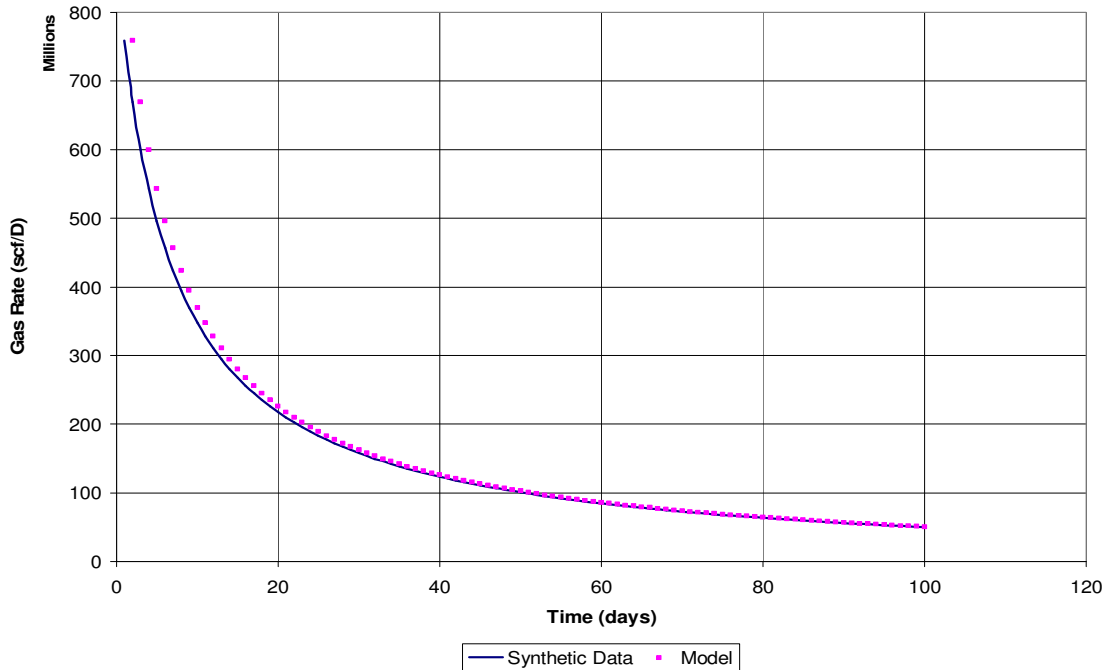
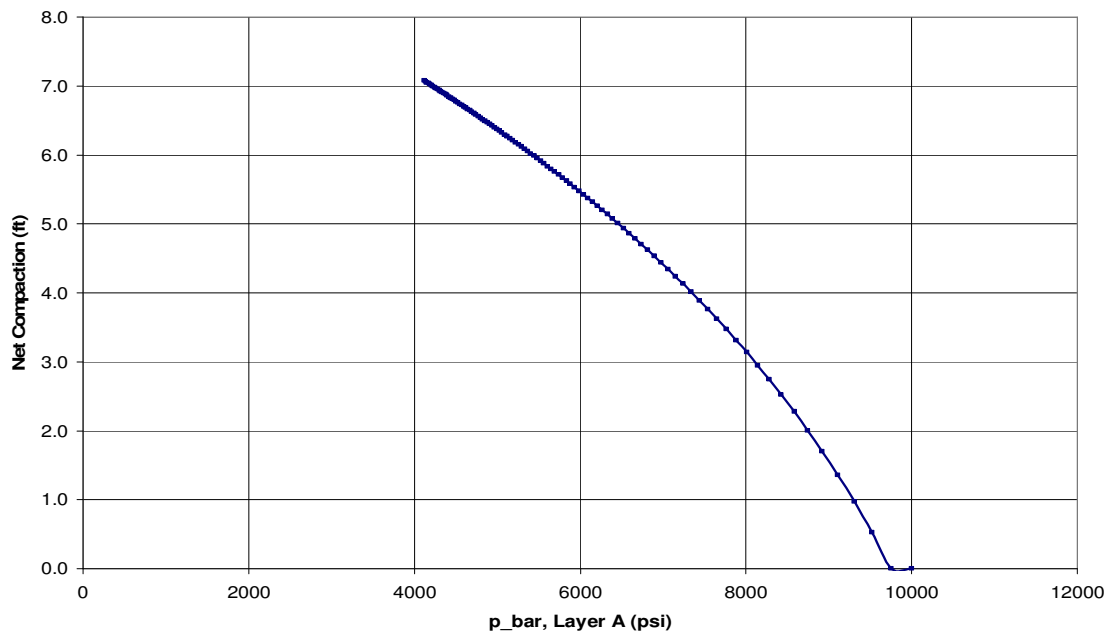
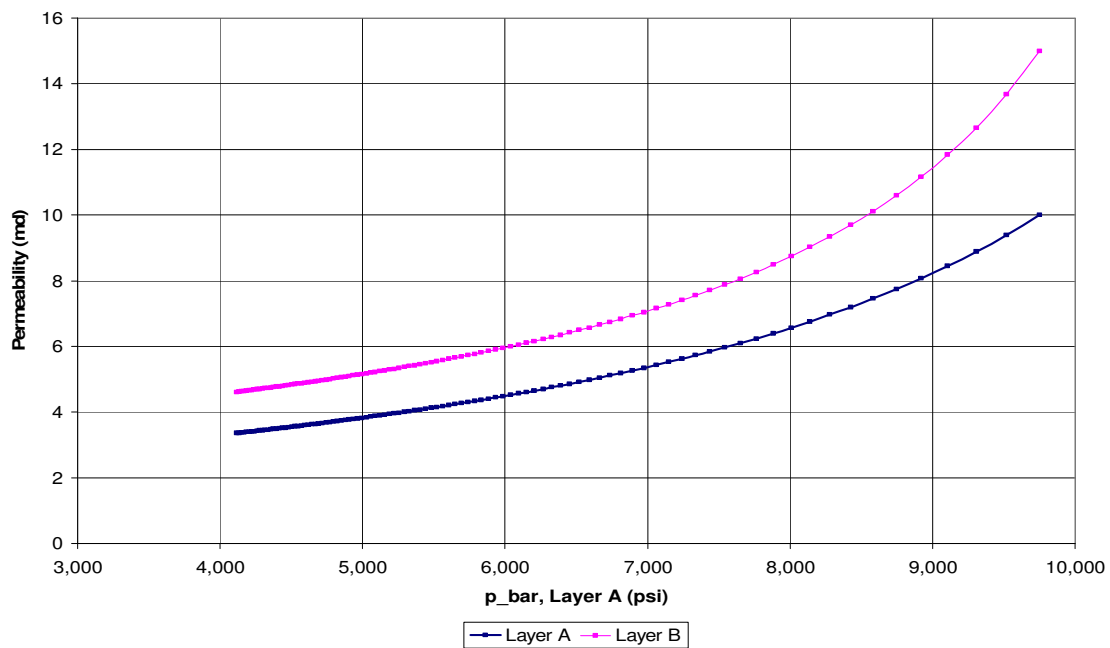
Fig. 4.13:  $q_g$  Vs  $T$  for 2-Layer Case A-B, after Optimization

Table 4.6: Results for unconsolidated 2-layer Case A-B						
	OGIP (MMscf)			$J_g$ (Mscf.cp/D/psi <sup>2</sup> )		
	Synthetic Data	Model	Error (%)	Synthetic Data	Model	Error (%)
A	11,267	11,529	2.3	$7.35 * 10^{-5}$	$7.56 * 10^{-5}$	2.9
B	16,900	16,638	1.6	$1.65 * 10^{-4}$	$1.63 * 10^{-4}$	1.3

Combined OGIP (MMscf):      Data: 28,167      Model: 28,167

Combined  $J_g$  (Mscf.cp/D/psi<sup>2</sup>):      Data:  $2.38 * 10^{-4}$       Model:  $2.38 * 10^{-4}$

## 2- Layer Case (A-B)

Fig. 4.14:  $dh$  Vs  $p_{bar}$  for 2-Layer Case A-B, after OptimizationFig. 4.15:  $k$  Vs  $p_{bar}$  for 2-Layer Case A-B, after Optimization

## 2- Layer Case (A-C)

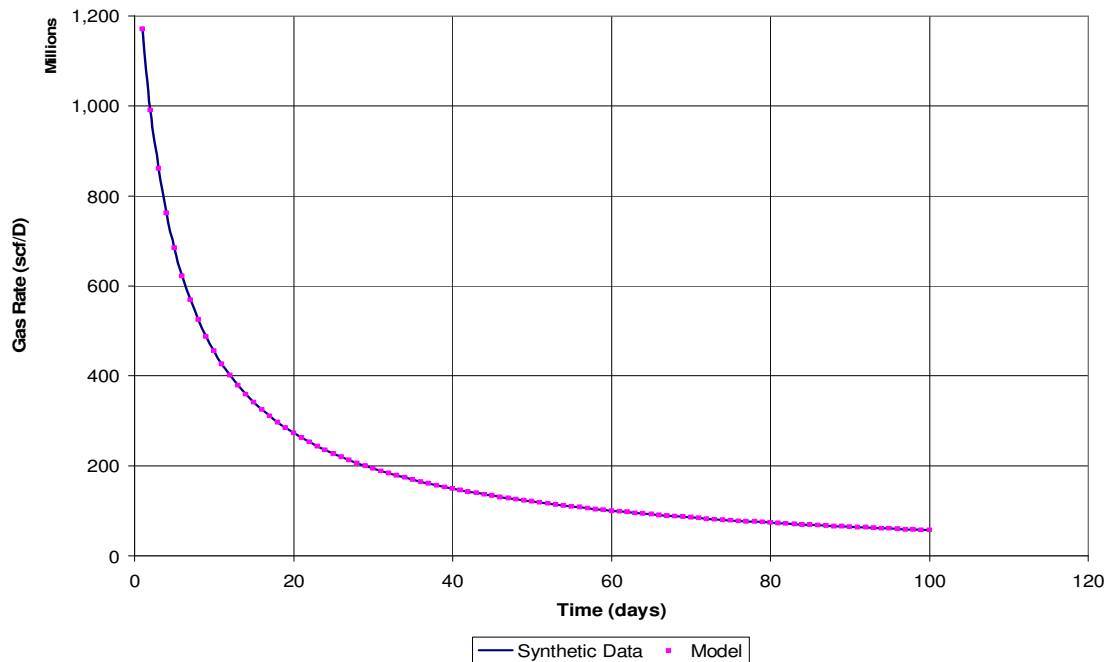
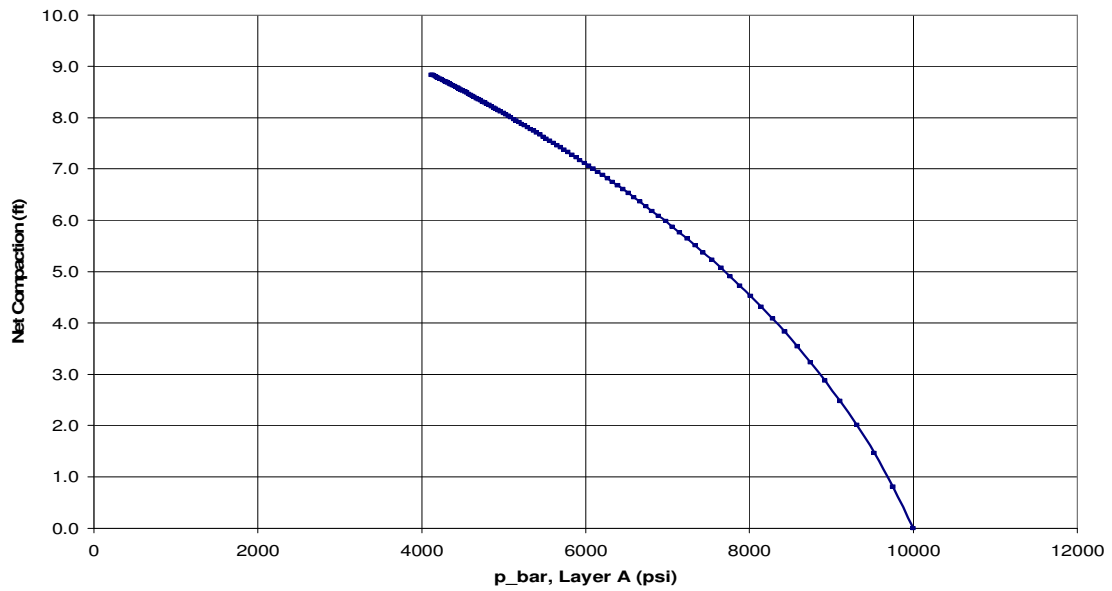
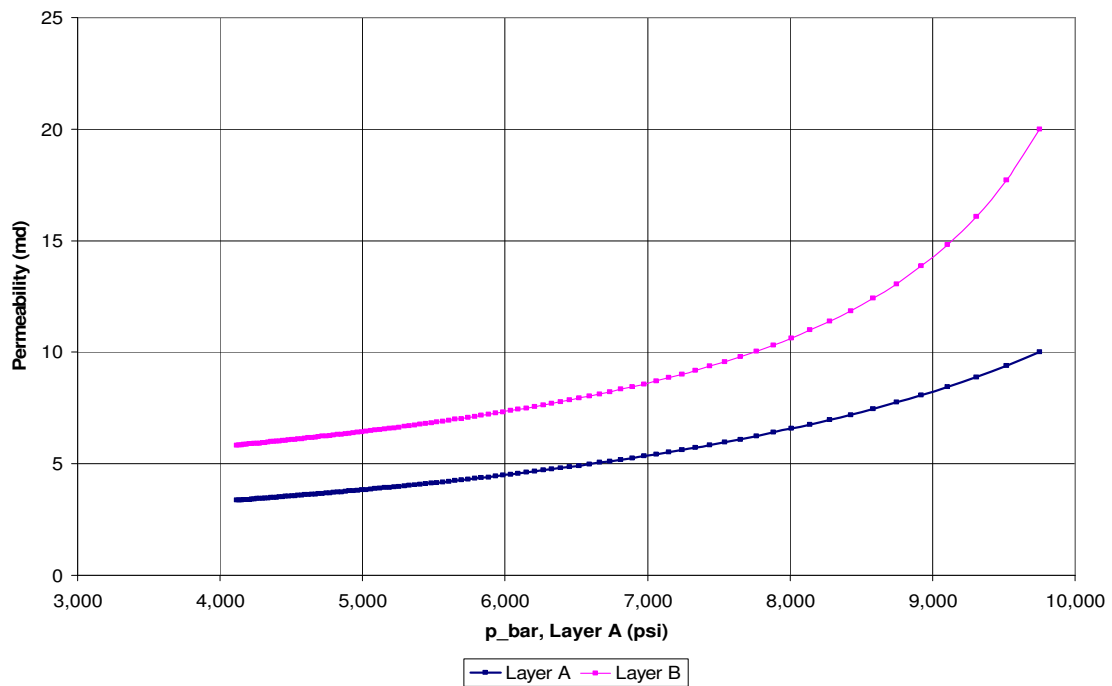
Fig. 4.16:  $q_g$  Vs  $T$  for 2-Layer Case A-C, after Optimization

Table 4.7: Results for unconsolidated 2-layer Case A-C						
	OGIP (MMscf)			$J_g$ (Mscf.cp/D/psi <sup>2</sup> )		
	Synthetic Data	Model	Error (%)	Synthetic Data	Model	Error (%)
A	11,267	11,384	1.0	$7.35 * 10^{-5}$	$7.46 * 10^{-5}$	1.5
C	22,533	22,415	0.5	$2.94 * 10^{-4}$	$2.93 * 10^{-4}$	0.4

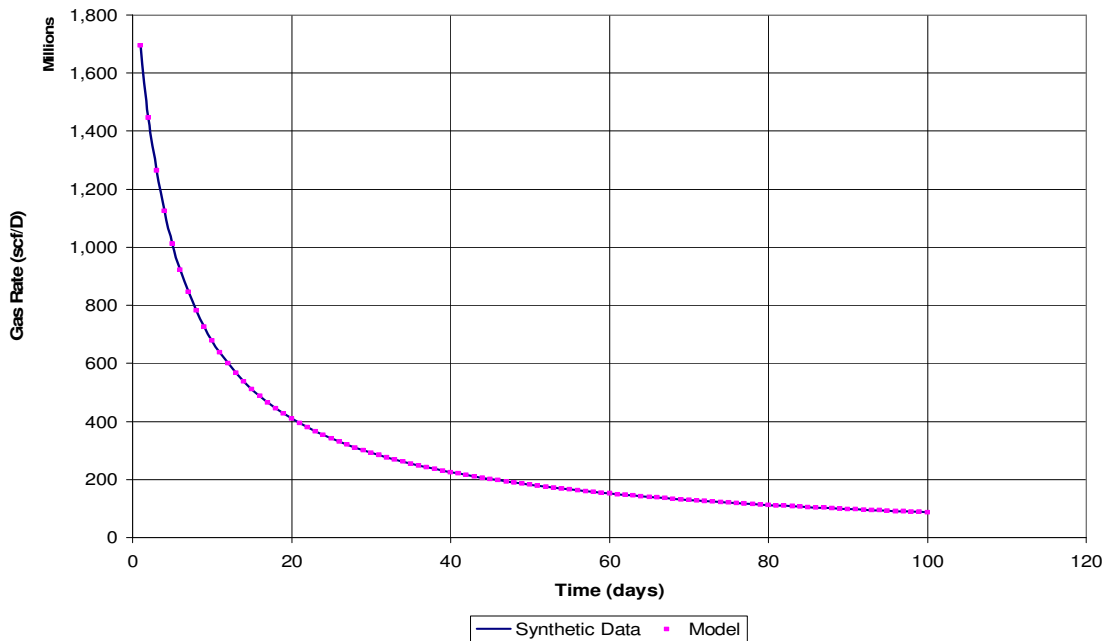
Combined OGIP (MMscf):            Data: 33,800            Model: 33,799

Combined  $J_g$  (Mscf.cp/D/psi<sup>2</sup>):    Data:  $3.68 * 10^{-4}$     Model:  $3.68 * 10^{-4}$

## 2- Layer Case (A-C)

Fig. 4.17:  $dh$  Vs  $\bar{p}$  for 2-Layer Case A-C, after OptimizationFig. 4.18:  $k$  Vs  $\bar{p}$  for 2-Layer Case A-C, after Optimization

## 3- Layer Case (A-B-C)

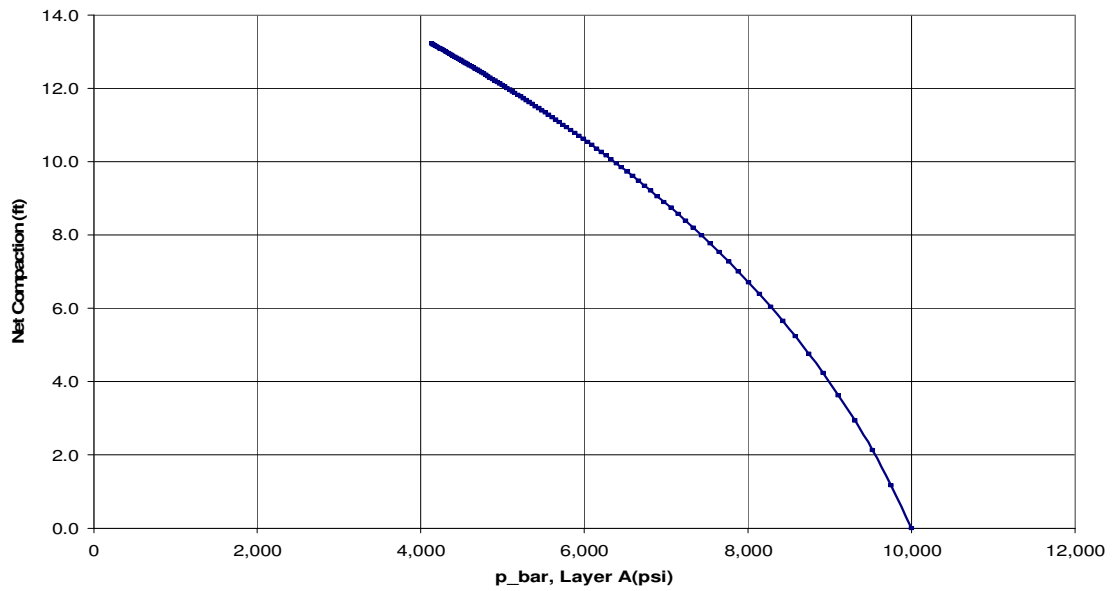
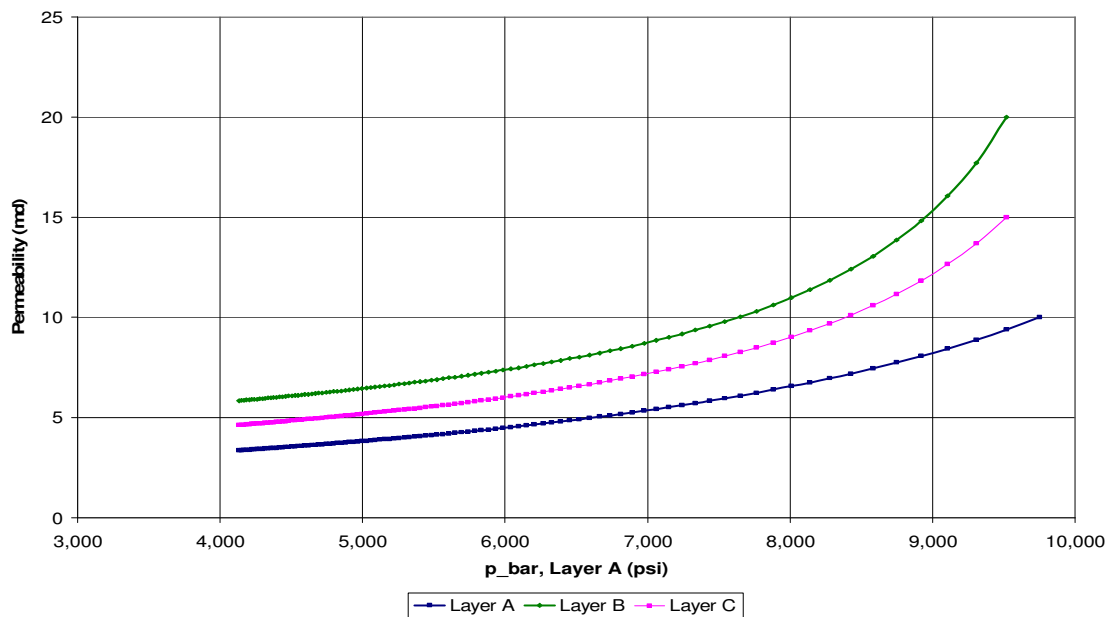
Fig. 4.19:  $q_g$  Vs  $T$  for 3-Layer Case A-B-C, after Optimization

	OGIP (MMscf)			$J_g$ (Mscf.cp/D/psi <sup>2</sup> )		
	Synthetic Data	Model	Error (%)	Synthetic Data	Model	Error (%)
A	11,267	8,535	24.2	$7.35 * 10^{-5}$	$5.36 * 10^{-5}$	26.9
B	16,900	16,963	0.4	$1.65 * 10^{-4}$	$1.53 * 10^{-4}$	7.2
C	22,533	25,201	11.8	$2.94 * 10^{-4}$	$3.26 * 10^{-4}$	10.7

Combined OGIP (MMscf):      Data: 50,700                      Model: 50,699

Combined  $J_g$  (Mscf.cp/D/psi<sup>2</sup>):      Data:  $5.32 * 10^{-4}$                       Model:  $5.32 * 10^{-4}$

## 3- Layer Case (A, B &amp; C)

Fig. 4.20:  $dh$  Vs  $p_{bar}$  for 3-Layer Case A-B-C, after OptimizationFig. 4.21:  $k$  Vs  $p_{bar}$  for 3-Layer Case A-B-C, after Optimization

## V. DISCUSSIONS

### 5.1 Status of Model

In chapter 2, a description of the variety of applications of the model was given which include: handling one well completed in one reservoir layer (section 2.3), one well completed in multiple reservoir layers (section 2.4) and multiple wells completed in multiple reservoir layers (section 2.5). As at the time of writing this thesis, the model has can be applied to both 2.3 and 2.4, but not section 2.5. A representation of the current application of the model is given in Fig. 4.1 which shows one well completed in multiple reservoir layers.

Table 5.1: Status of Depletion Model

Reservoirs	OGIP <sub>1</sub>	OGIP <sub>2</sub>	OGIP <sub>3</sub>	OGIP <sub>4</sub>
Wells				
n <sub>well</sub> = 1	✓	✓	✓	✓

### 5.2 Limitation of Model

An attempt to match the model with more than three layers did not always converge to good estimated values of both *OGIP* and *J<sub>g</sub>*. Comparable results were only possible if good initial estimates were chosen or if one set of parameters (i.e. either *OGIP* or *J<sub>g</sub>*) were known. In running the model, it was notice the more complexity of the reservoir determines the importance of the initial estimates of Gas in Place and Productivity Index (OGIP<sub>guess</sub> and J<sub>g\_guess</sub>) supplied to the model. For one-layer cases the

model always converges to the right values *OGIP* and Productivity Index irrespective of the initial estimates supplied. For two layer cases, initial estimates of five times higher or lower than accurate values were tried successfully. For three layers and above, better estimates had to be supplied for good convergence of the results.

### 5.3 Timeframe of Production Data

To reduce multi-layered calculations to a summation of individual production rate for each layer, the model assumes a constant FBHP for all layers. The model therefore calculates a very high rate from the onset of each run especially considering an initial reservoir pressure of 10,000 psi for deep water cases. In order to obtain multiple data points as well as a consistent plot profile, daily production rate was used in both consolidated and unconsolidated case (Chapters 3 and 4). Compaction and permeability retardation results shown in this project would therefore typically occur over a larger timeframe (i.e. years) in the field corresponding to the time required for the accompanied pressure depletion shown in each case. For field applications, the model should be run in the monthly production data mode since most data are measured monthly.

## VI. CONCLUSIONS AND RECOMMENDATIONS

### 6.1 Conclusions

Since formation compressibility is unique for each rock type, by developing a set of equations using Yale's correlation for formation compressibility, gas depletion equation, pseudo-steady state equation and Geomechanics calculations a general Compartmentalized model that applies to all rock types can be developed. The Compartmentalized Depletion model can be used to analyze production data from multi-layered reservoirs. The model is applicable to both consolidated and unconsolidated reservoirs and gives good estimates of OGIP and Productivity Index for each layer.

For conventional consolidated gas reservoir with low to high permeability cases, results from the model compares well with that a gas Simulator. OGIP are however underestimated if transient data is included in the analysis. For unconsolidated gas reservoirs, reduction in permeability and reservoir compaction could be very significant especially for reservoirs with large pay thickness and large depletion pressure. By including the appropriate permeability decrease with depletion, the model gives a more realistic forecast for production from an unconsolidated deep water reservoir.

The model gives an estimate of reservoir compaction with time which can aid in selection of the right tubular that can withstand the accompanied stress thereby preventing casing or tubing collapse.

## 6.2 Recommendations

The optimization routine used was set up using Microsoft Solver. The advantage is that it is available to all Microsoft Excel users. This software is credited be able to solve for several hundred variables but only worked efficiently for six variables (three-layer case) in this work. It should be interesting to find out if it could be possible to re-organize the equations in a way that would optimally use the performance of Excel Solver. Alternatively, a better optimization routine could also be written or sourced-for to make the model applicable to more than three layers.

With a more efficient optimization routine that could solve for more variables, the model could be set up to include communication among compartments ( $C_{ires,ires}$ ). It could also be possible to solve for a field case with several wells each completed in several layers (i.e. many optimization variables).

In this work, non Darcy flow effect was neglected. Though this assumption is not of much significance with low permeability gas reservoirs, it is important in high permeability (hence high rate) wells. The model should therefore be updated to include non Darcy effect. Including transient flow in addition to pseudo steady state flow could also be added to the model. Field data was not available for comparison during this work. A test using field data would be very helpful in calibrating the model.

## NOMENCLATURE

$\alpha$	Biot's constant
$A, B, C, D$	Yale's Factors for Calculating Variable Compressibility
<i>Area</i>	Reservoir Area (ft <sup>2</sup> )
$b$	Arp's Decline Curve Exponent
$B_g$	Reservoir Gas Formation Volume Factor (rft <sup>3</sup> /scf)
$D_g$	Non-Darcy Flow Coefficient (Mscf/D) <sup>-1</sup>
$C_A$	Reservoir Shape factor
$C$	Cross Flow Coefficient (MMscf/psi <sup>2</sup> /cp)
$c_b$	Bulk Volume Compressibility (1/psi)
$c_\phi$	Pore Volume Compressibility, commonly called formation compressibility (1/psi)
$c_{bm}$	Uniaxial Bulk Volume Compressibility (1/psi)
$c_{\phi m}$	Uniaxial Pore Volume Compressibility (1/psi)
$c_r$	Rock or Grain Compressibility (1/psi)
$c_t$	Total Compressibility (1/psi)
$e_{r1} / e_{r2} / e_{r3}$	Difference between Measured or Simulated Data and Model Calculation before Optimization for One Layer Case, Multiple Layer Case or Entire Field.
$\phi$	Porosity
$G_p$	Cumulative Gas Produced (MMscf)
$h$	Formation Height (ft)
$i_{res}$	Each Compartment in the Reservoir
$i_{well}$	Each Well in the Field.

$J_g$	Productivity Index (MMscf/psi <sup>2</sup> /cp)
$k$	Permeability (md)
$K_1, K_2, K_3$	Yale's Factors for Calculating Variable Compressibility
$\lambda$	Carter's Dimensionless Variable
$m$	Permeability-to-Porosity Exponent
$\mu$	Viscosity (cp)
$m(p)$	Pseudo pressure (psi <sup>2</sup> /cp)
$n_{res}$	Total Number of Compartments in the Reservoir
$n_{well}$	Total Number of Wells in the Field
$n_{time}$	Number of Time Steps
$OGIP$	Original Gas in Place (Bscf)
$ovb$	Overburden Pressure (psi)
$p_{bar}$	Average Reservoir Pressure (psi)
$p_{wf}$	Flowing Bottom Hole pressure (psi)
$q_g$	Gas Rate (MMscf/day)
$r_d$	Drainage Radius (ft)
$r_e$	Outer Boundary Radius (ft)
$r_w$	Well Radius (ft)
$S$	Saturation
$s$	Skin
$\sigma_e$	Effective Stress (psi)
$\sigma_c$	Compressive / Laboratory Stress (psi)

$\sigma_p$	Stress Due To Reservoir Pressure (psi)
$t$	Time (days)
$t_{pps}$	Time To Reach Pseudo-steady State (days)
$T$	Reservoir Temperature ( $^{\circ}$ Rankine)
$V$	Volume
$Z$	Gas Compressibility Factor
Subscripts	
$1$	First Layer Properties
$2$	Second Layer Properties
$data$	Measured / Simulated Property
$g$	Gas
$guess$	Initial Value of Reservoir Property Supplied by User Before Optimization
$i$	Initial
$o$	Oil
$model$	Property Calculated by the Model
$p$	Formation Pore
$sc$	Standard Conditions (e.g. temperature, pressure etc)
$t$	Total
$w$	Water
Superscript	
$n$	Each Time step

## REFERENCE

1. Yale, D.P., Nabor, G.W., Russell, J.A., Pham, H.D. and Yousef, M.: "Application of Variable Formation Compressibility for Improved Reservoir Analysis," paper SPE 26647 presented at the SPE Annual Technical Conference and Exhibition, Houston, Texas, Oct. 3-6.
2. Sawabani, C.T. and Chilinger, G.V.: "Compressibility of Unconsolidated Arkosic Oil Sands," Paper SPE 40SIJ was presented at 1972 SPE-AIME 47th Annual Fall Meeting, held in San Antonio, Texas, Oct. 8-11.
3. Geertsma, J.: "Land Subsidence above Compacting Oil and Gas Reservoirs," *JPT* (June 1973) 734-744.
4. Ostermeier, R.M.: "Compaction Effects on Porosity and Permeability: Deepwater Gulf of Mexico Turbidities," *JPT* (Feb. 2001) **53**, 68 - 74.
5. Ostermeier, R.M.: "Stressed Oil Permeability of Deepwater Gulf of Mexico Turbidite Sands: Measurement and Theory," *SPEFE* (Oct. 1996), 229-235.
6. Settari, A.: "Reservoir Compaction," *JPT* (Aug. 2002) **54**, 62-69.
7. Gray, D.H., Fatt, I. and Bergamini, G.: "The Effect of Stress on Permeability of Sandstone Cores," *SPEJ* (June 1963) 95-100; Trans., AIME 228.
8. Fredrick, J.T., Arguello, J.G, and Deitrick, G.L.: "Geomechanical Modeling of Reservoir Compaction, Surface Subsidence, and Casing Damage at the Belridge Diatomite Field," *SPEREE* (Aug. 2000) **3**, 348-359.

9. Schutjens, P.M.T.M., Hanssen, T.H., Hettema, M.H.H., and Merour, J.: “Compaction-Induced Porosity / Permeability Reduction in Sandstone Reservoirs: Data and Model for Elasticity-Dominated Deformation,” *SPEEE* (June 2004) **7**, 202-216.
10. Lee, J. and Wattenbarger, R.A.: *Gas Reservoir Engineering*, SPE, Richardson, TX (2004).
11. F’etkovich, M. J.: “Decline Curve Analysis Using Type Curves,” *JPT* (June 1980) 1065 - 1077.
12. Carter, R D.: “Type Curves for Finite Radial and Linear Gas-Flow Systems: Constant-Terminal-Pressure Case,” *SPEJ* (1985)719 – 28.
13. E1-Banbi, A.H.: *Layered Pseudo-Steady-State Models for Tight Commingled Gas Reservoir*, MS Thesis, Texas A&M University, College Station, Texas (May 1995).
14. E1-Banbi, A.H. and Wattenbarger, R.A.: “Analysis of Commingled Tight Gas Reservoirs,” paper SPE 36736 presented at the 1996 SPE Annual Technical Conference and Exhibition held in Denver, Colorado, Oct. 6-9.
15. E1-Banbi, A.H. and Wattenbarger, R.A.: “Analysis of Commingled Gas Reservoirs with Variable Bottom-Hole Flowing Pressure and Non-Darcy Flow,” paper SPE 38866 prepared for presented at the 1997 SPE Annual Technical Conference and Exhibition held in San Antonio, TX, Oct. 5-8.
16. Arevalo-Villagran, J.A., E1-Banbi, A.H. and Wattenbarger, R.A.: “Production Analysis of Commingled Gas Reservoirs – Case Histories,” paper SPE 58985

presented at the 2000 SPE Annual Technical Conference and Exhibition held in Mexico, Feb. 1-3.

17. Settari, A.T. and Walters, D.A.: “Advances in Coupled Geomechanical and Reservoir Modeling with Applications to Reservoir Compaction,” paper SPE 51927 presented at the 1999 SPE Reservoir Simulation Symposium, Houston, Texas, February 14-17.
18. Dean, R.H., Gai, X., Stone, C.M. and Minkoff, S.E.: “A Comparison of Techniques for Coupling Porous Flow and Geomechanics,” *SPEJ* (2006)132 – 140.
19. Settari, A.T., Bachman, R.C. and Walters, D.A.: “How To Approximate Effects of Geomechanics in Conventional Reservoir Simulation,” paper SPE 97155 presented at the 2005 SPE Annual Technical Conference & Exhibition, Dallas, Texas, Oct. 9-12.
20. Biot, M.A.: “General Theory of Three Dimensional Consolidation,” *App. Phy.* (1941) **12**, 155-164.
21. Biot, M.A.: “Theory of Elasticity and Consolidation for a Porous Anisotropic Solid,” *App. Pby.* (1955) **26**, 182-185.
22. Geertsma, J.: “The effect of Fluid Pressure Decline on Volumetric changes of Porous Rocks”, *Trans. AIME*, 339, 1957.
23. Nur, A. and Byerlee, J.D.: “An Exact Effective Law for Elastic Deformation of Rock with Fluids”, *Journal of Geophysical Research* (Sept. 1971) **76**, 6414 - 6419.
24. Teeuw, D.K.: “Prediction of Formation Compaction from Laboratory Compressibility Data” *SPEJ* (Sept. 1971) 263 – 271.

25. Mattax, C.C., McKinley, R.M. and Clothier, A.T.: “Core Analysis of Unconsolidated and Friable Sands”, *JPT* (Dec. 1975) 1423 – 1432.
26. Holditch, S.A. and Zillur, R.: “Developing Data Sets for 3D Fracture Propagation Models,” *SPEPF* (Nov. 1994) 257 – 261.
27. Al-Hussainy, R., Ramey, H.J., and Crawford, P.B.: “The Flow of Real Gases through Porous Media,” (May 1966), 624-636; Trans., AIME 237.
28. Dake, L.P.: *Fundamentals of Reservoir Engineering*, Elsevier Scientific Publishing Co., Amsterdam (1978).
29. Economides, M.J., Hill, A.D. and Economides, C.E.: *Petroleum Production Systems*, Prentice Hall, Inc., NJ (1994).
30. Poston, S.W. and Berg, R.R.: *Overpressured Gas Reservoirs*, SPE, Richardson, Texas (2002).
31. Zimmerman, R.W.: *Compressibility of Sandstones*, Development in Petroleum Science, 29, Elsevier, 1991.

## APPENDIX A: Basic Geomechanics

Compaction is the reduction in pore volume due to a change in reservoir pressure while subsidence is the movement of surface strata in response to a loss of underground support often associated with reservoir compaction due to hydrocarbon withdrawal.

### Mechanism of Compaction

The weight of sediments overlying a producing horizon is supported partially by the rock matrix and partially by the fluid pressure within the rock pore space. As fluids are withdrawn and pressure depletes, more of the load is transferred to the rock matrix and producing formation compacts. Conditions which may lead to significant compaction and subsidence problems include: soft formation materials, large pressure decline and large producing interval. Effects of Reservoir compaction include: casing collapse, well failure, porosity and permeability reduction.

In the subsurface, the overburden stress is the summation of the initial effective vertical stress exerted on the rock matrix ( $\sigma_{ei}$ ) and the initial reservoir pore pressure ( $p_i$ ). In geo-pressure formations, high reservoir pressure implies a lower effective stress thereby a weaker formation rock. Before production, these stresses are balanced<sup>30</sup> as given in Eq A.1 and depicted in Figure A.1.

$$\sigma_t = \sigma_{ei} + p_i \quad \text{A.1}$$

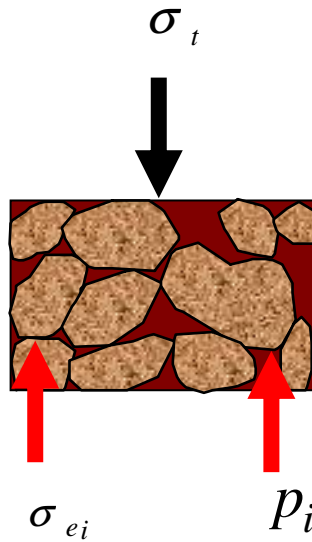


Figure A.1: Stress / Pressure Balance on Formation before Production

During hydrocarbon production, the total overburden stress remains the same (Eq. A.2), there is a reduction in average reservoir pressure to a new value of  $p_n$  leading to an increase in the effective vertical stress (Eq. A.4). The new value of effective vertical stress is given by Eq. A.3. For a reservoir with high formation compressibility, this increase in effective vertical stress leads to deformation of the reservoir in the vertical direction.

$$\sigma_t = \sigma_{en} + p_n \quad \text{A.2}$$

$$\sigma_{en} = \sigma_e + \alpha^* (p_i - p_n) \quad \text{A.3}$$

$$\Delta\sigma_e = \alpha^* (p_i - p_n) \quad \text{A.4}$$

Where  $\alpha$  is the Biot's constant given by Eq. 1.3

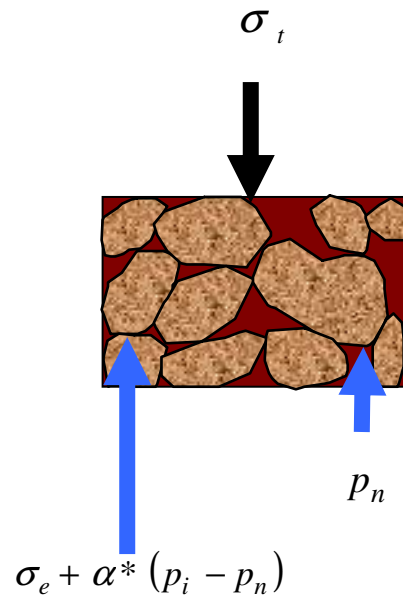


Figure A.2: Stress / Pressure Balance on Formation during Production

Provided lateral dimensions are large compared with their height, reservoir deform predominantly in the vertical plane<sup>3</sup>. Formation compaction can therefore be characterized by a Uniaxial Compaction Coefficient, which expresses the change in height (relative to the initial height) caused by an increase in effective stress ( $\Delta\sigma_e$ ) due to a reduction in reservoir pressure, under constant overburden. Using the definition of Geertsma<sup>3</sup> a *Uniaxial Compaction Coefficient*,  $c_{bm}$ , is then be defined. The corresponding equation when estimating uniaxial compaction coefficient from change in laboratory stress is given by Eq. A.5b. The multiplying constant from

reservoir pressure change to laboratory pressure / stress change (Biot's constant  $\alpha$ ) reduces to a value of 1 if the rock grain compressibility is negligible in comparison with bulk compressibility.

$$c_{bm} = \frac{1}{z} \frac{dz}{dp} \quad \text{A.5}$$

$$c_{bm} = \frac{1}{z} \frac{dz}{\alpha d\sigma_{lab}} \quad \text{A.5b}$$

The total reduction in reservoir height can then be expressed as <sup>3</sup>:

$$\Delta h = \int_{p_i}^{p_{nime}} h(p) * c_{bm}(p) dp \quad \text{A.6}$$

## APPENDIX B: Measurement of Variable Formation Compressibility

## Oedometer Test

As discussed, in Appendix A, the most important parameter in making compaction calculation is the uniaxial bulk compressibility. This rock property is typically measured in the laboratory using the Oedometer test<sup>24</sup> (Fig. B.1). The test simulates reservoir boundary condition of zero lateral displacement. Because of the difficulty associated with conducting this test (measurement errors, cost of test, requirement of core to fit exactly in the cell), this rock property is often estimated from an easier test: the hydrostatic test.

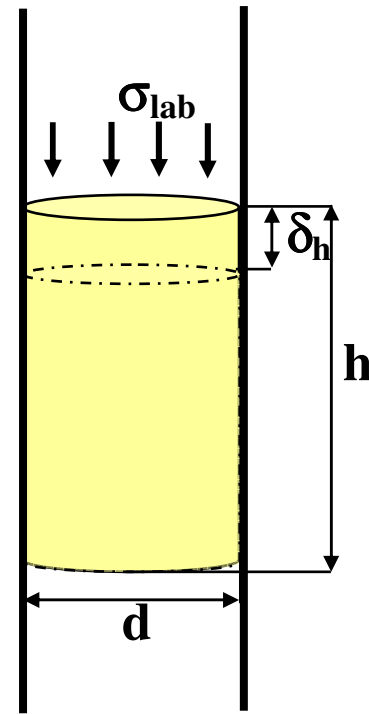


Fig. B.1 Oedometer test

### Hydrostatic Test

Rock pore volume compressibility (often referred to as formation compressibility) is measured using the hydrostatic test<sup>24</sup> (shown in Figure B.2). The core is filled with brine or air at atmospheric pressure, and subjected to hydrostatic stress (Fig. B.2). The change in pore volume is estimated by measuring the volume of fluid ejected from the core. The pore (or formation) compressibility is then calculated using Eq. B.1. Equation B.2 employs a correction factor which reduces the 3-D deformation measured in pore volume compressibility ( $c_\phi$ ) to a 1-D uniaxial compressibility ( $c_{\phi m}$ ).

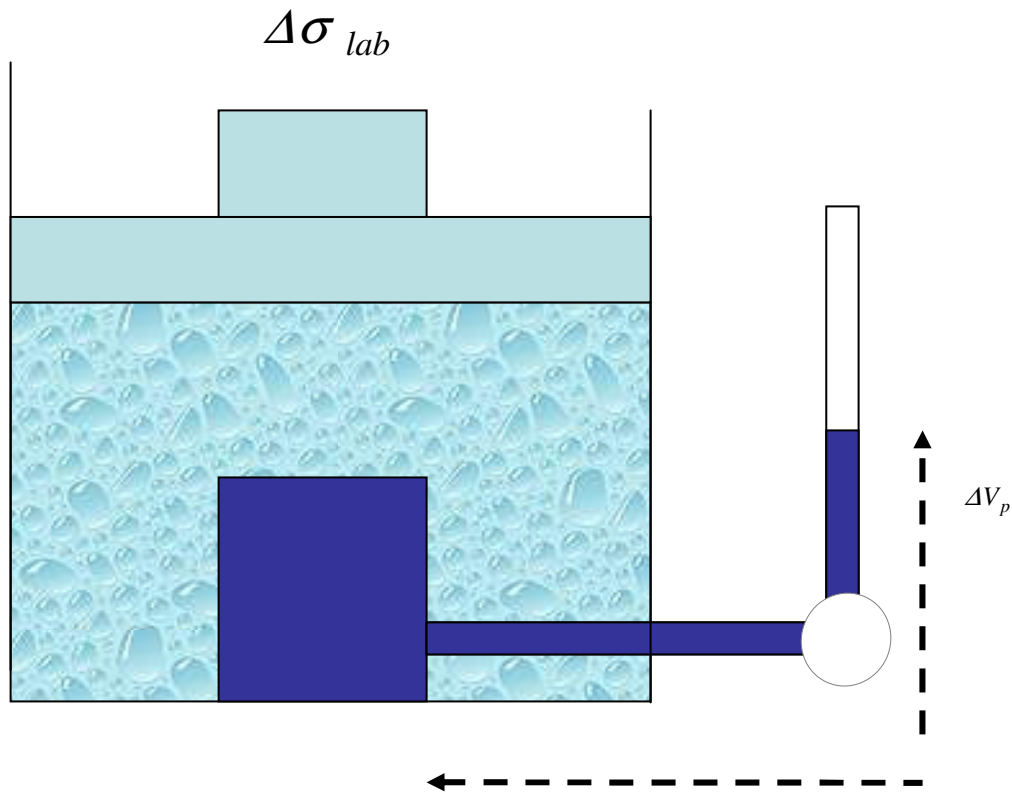


Fig. B.2 Hydrostatic test

$$c_{\phi} = \frac{\Delta V_p / V_p}{\Delta \sigma_{hyd}} \quad \text{B.1}$$

$$c_{\phi_m} = \frac{1}{3} \left( \frac{1+\nu}{1-\nu} \right) \alpha c_{\phi} \quad \text{B.2}$$

Yale *et al*<sup>1</sup> conducted hydrostatic tests on a number of samples from different reservoir rocks, applied the correction factor and came up with a correlation that describes uniaxial pore volume compressibility for reservoir rock with pressure. This correlation was used in this project in the absence of laboratory measurements.

Bulk volume compressibility is related to the pore volume compressibility using equation B.3<sup>31</sup> while the corrected form of the equation (using uniaxial correction factor) is given in B.4. The uniaxial bulk volume compressibility is used for compaction calculations.

$$c_b = \phi * c_{\phi} \quad \text{B.3}$$

$$c_{bm} = \phi * c_{\phi_m} \quad \text{B.4}$$



## VITA

Name: Nurudeen Yusuf

Address: 35, Ikale Street, Papa Ajao, Mushin, Lagos, Nigeria

Email Address: nxyusuf@yahoo.com

Education: B.S., Mechanical Engineering, University of Lagos, Nigeria, 1999.  
M.S. Petroleum Engineering, Texas A&M University, 2007  
University, 2005.